

# Correlation-enhanced electron-phonon coupling: Applications of GW and *screened* hybrid functional to bismuthates, chloronitrides, and other high $T_C$ superconductors

Z. P. Yin,\* A. Kutepov, and G. Kotliar

*Department of Physics and Astronomy, Rutgers University, Piscataway, New Jersey 08854, United States.*

(Dated: November 27, 2024)

We show that the electron-phonon coupling (EPC) in many materials can be significantly underestimated by the standard density functional theory (DFT) in the local density approximation (LDA) due to large non-local correlation effects. We present a simple yet efficient methodology to evaluate the realistic EPC going beyond LDA by using more advanced and accurate GW and *screened* hybrid functional DFT approaches. The corrections we propose explain the extraordinarily high superconducting temperatures that are observed in two distinct classes of compounds—the bismuthates and the transition metal chloronitrides, thus solving a thirty-year-old puzzle. Our work calls for the critically reevaluation of the EPC of certain phonon modes in many other materials such as cuprates and iron-based superconductors. The proposed methodology can be used to design new correlation-enhanced high temperature superconductors and other functional materials involving electron-phonon interaction.

## I. INTRODUCTION

The microscopic origin of superconductivity has been established in numerous classes of materials. In conventional superconductors such as elemental metals it results from the exchange of phonons. In the copper oxides, the iron pnictides and some organic compounds, superconductivity is connected to close proximity to a magnetic state. On the other hand, the cause of superconductivity in a large third class of high temperature superconductors including  $\text{Ba}_{1-x}\text{K}_x\text{BiO}_3$  ( $T_{c,max} \simeq 32$  K)<sup>1</sup>, electron-doped  $\beta\text{-HfNCI}$  compounds ( $T_{c,max} \simeq 25.5$  K)<sup>2</sup>, and alkali-doped fullerenes  $A_3\text{C}_{60}$  ( $T_{c,max}$  up to 40 K)<sup>3</sup> is still mysterious. They have been referred to as the “other high-temperature superconductors”,<sup>4,5</sup> because neither spin nor phonon seems to be responsible for their high superconducting temperatures.

Since they are apparently diamagnetic (thus the spin degree of freedom seems irrelevant), two charge mediated pairing mechanisms have been proposed (and ruled out) for the bismuthates: the “negative U” scenario<sup>6,7</sup> and strong coupling to an O-breathing phonon mode<sup>8,9</sup>. The first scenario involves the tendency of Bi atoms to avoid the  $\text{Bi}^{4+}$  state, while preferring the  $\text{Bi}^{3+}$  and  $\text{Bi}^{5+}$  charge state, thus generating an attractive local “negative U” pairing center. However, first principles calculations have so far ruled out the negative U mechanism<sup>10,11</sup>. Regarding the electron-phonon mechanism, previous approaches to the *ab initio* evaluation of the electron-phonon coupling (EPC) were based on the density functional theory (DFT) and linear response theory (LRT)<sup>12</sup> in the local density approximation (LDA) or generalized gradient approximation (GGA). The EPC calculated by this standard DFT-LDA/GGA approach is insufficient to account for the high  $T_c$  in both  $\text{Ba}_{1-x}\text{K}_x\text{BiO}_3$ <sup>13</sup> and the electron-doped transition metal chloronitrides<sup>14,15</sup> within the Migdal-Eliashberg theory, which seems to rule out the phonon mechanism.

However, to rule out the phonon mechanism, the EPC has to be evaluated reliably. It is well-known that the

standard DFT-LDA approach fails to describe well the electronic structure of strongly correlated materials. This rises the question whether the EPC is properly treated by the standard DFT-LDA approach for the “other high temperature superconductors”<sup>4,5</sup> and other correlated materials in general. Despite the answer to this question, a reliable evaluation of electron-phonon interaction (EPI) strength for real materials is of fundamental importance for both understanding the underlying physics and designing novel functional materials. (The EPC for metallic materials is the average EPI matrix elements on the Fermi surface.) The EPI/EPC plays an important role not only in conventional superconductivity, but also in electronic transport, electronic-heat capacity, etc. Even in the cuprate superconductors, there are evidences<sup>16–19</sup> (see also Ref.20 for a review) that EPC is strong and may play an important role in the unconventional superconductivity<sup>18</sup>.

The EPC for materials can be estimated by both experimental techniques and theoretical methods. Experimentally, its strength can be estimated by means of neutron scattering<sup>21</sup>, Raman scattering<sup>22</sup>, tunneling<sup>23</sup> and photoemission<sup>18</sup>. However these experiments are usually limited to be able to estimate the EPC strength for only a few phonon modes.<sup>18,22,24,25</sup> Theoretically, first principle calculations based on density functional theory and linear response technique, on the other hand, can provide a complete evaluation of the EPI including all phonon modes, and is widely used for calculating lattice dynamical properties and EPC of solids. For example, the EPC evaluated by this approach with LDA/GGA are strong enough to account for the rather high temperature superconductivity in *conventional* superconductors such as elemental lithium ( $T_c \sim 20$  K)<sup>26</sup>, yttrium ( $T_c \sim 20$  K)<sup>27</sup>, calcium ( $T_c \sim 25$  K)<sup>28</sup> and binary compound  $\text{MgB}_2$  ( $T_c \sim 40$  K)<sup>29</sup>. This recorded success of LDA linear response calculations for conventional superconductors gives rise to the puzzles about the mechanism of superconductivity in the “other high temperature superconductors” including the bismuthates and the transition metal chloronitrides

as mentioned above.

In this paper, we show that these “other high temperature superconductors” are strongly coupled superconductors where the coupling of the electrons to the lattice vibrations are strongly enhanced by correlation effects which requires treatments of electron-electron interaction beyond LDA/GGA. Once the EPC is properly evaluated, it is strong enough to account for their high temperature superconductivity. Our view is supported by various experiments which show strong EPC for certain phonon modes of these superconductors.<sup>30–33</sup>

The key is to overcome the overscreening problem of LDA/GGA and achieve a simultaneous faithful description of the ground state electronic structures and lattice dynamical properties. We will show that an appropriate screened hybrid functional and quasi-particle GW (QPGW) method provide an accurate description of the normal state electronic structures, and can be combined with linear response approach to accurately determine lattice dynamical properties and the EPC of these materials. The problem is that the GW method and the screened hybrid functional approach are very computationally demanding, combining them directly to linear response approach pose a serious challenge to nowadays technology. It is therefore desirable to have a simplified method to estimate the EPC strength to a reasonable accuracy.

To this end, we propose such a method based on LDA linear response calculations and a few GW and/or screened hybrid functional supercell calculations. The latter are used to replace the most important electron-phonon matrix elements in the LDA linear response calculations to obtain an improved evaluation of the EPC. We apply our method to the (Ba,K)BiO<sub>3</sub> and electron-doped HfNCI high temperature superconductors and find that the EPC computed by our method are significantly enhanced compared to the values predicted by LDA linear response calculations and are strong enough to account for the experimental  $T_c$  in these materials within the standard Migdal-Eliashberg theory. Therefore the puzzling high temperature superconductivity in this class of superconductors is naturally explained. In addition, our method explains the material and doping dependence of  $T_c$  in these superconductors and related compounds. Our method can also be used to design new high temperature superconductors and other EPI/EPC related functional materials.

This paper is organized as following: we first clarify two sources of electronic correlations starting from LDA and their impacts on lattice dynamic properties (section II). A general understanding of the EPC and our method to estimate the EPC combining LDA linear response calculations and GW/screened hybrid supercell calculations is presented in section III. Section IV summarizes our computational details. The electronic structures, selected important phonon frequencies and EPC calculated by LDA functional, the screened hybrid functional, and QPGW approach are presented for (Ba,K)BiO<sub>3</sub> materials

in Section V and electron doped HfNCI/ZrNCI materials in section VI. A short summary is provided in Section VII followed by discussions. The paper is concluded in Section VIII.

## II. ELECTRONIC CORRELATION AND ITS IMPACT ON LATTICE DYNAMIC PROPERTIES

The frequency and momentum resolved green’s function  $G(\omega, k)$  can be written as  $G(\omega, k) = 1/(\omega - H(k)_{\text{meanfield}} - \Sigma(\omega, k))$  where  $H(k)_{\text{meanfield}}$  is some mean field Hamiltonian and  $\Sigma(\omega, k)$  is the self-energy correction induced by correlation effects. Naturally  $\Sigma(\omega, k)$  depends on the choice of the mean field method, thus the term “*correlation*”. Chemists usually use Hartree-Fock method as the mean field whereas many physicists prefer LDA/GGA within the DFT framework as the starting point. Here we adopt the physicists’ choice, i.e.,  $H(k)_{\text{meanfield}} = H(k)_{\text{DFT-LDA/GGA}}$ , and define correlation with respect to deviations from DFT-LDA/GGA. With this choice, the degree of correlation is quantified by  $\Sigma(\omega, k)$ .

When  $\Sigma(\omega, k)$  is negligible, the correlation is weak and static mean field theory such as DFT-LDA/GGA is reasonably accurate, for examples, Cu and Au. However, when  $\Sigma(\omega, k)$  is large, correlation is strong and has to be treated by approaches beyond DFT-LDA/GGA. There are different cases where the correlation can be taken into account by different methods.

If  $\Sigma(\omega, k)$  is dominated by the frequency dependence, the correlation is mainly local and is caused by the degeneracy error of LDA/GGA.<sup>34</sup> This local correlation is addressed by dynamical mean field theory (DMFT) combined with DFT-LDA/GGA.<sup>35,36</sup>

On the other hand, if  $\Sigma(\omega, k)$  has mostly the momentum dependence, the correlation is mostly non-local and is rooted in the semi-local nature of LDA/GGA which neglects the long-range exchange interaction. This non-local correlation can be accounted for by including long-range exchange interactions. GW method is able to determine the range of the exchange potential self-consistently and is suited to deal with the non-local correlation. The disadvantage is that GW calculations are often very computationally demanding. The most economical way to incorporate the long-range exchange interaction (non-local correlation) is by replacing the LDA/GGA functional by a *screened* hybrid functional<sup>37</sup>, such as HSE06<sup>38</sup>, which increases the spatial non-locality of the exchange potential relative to the LDA/GGA. The downside of the screened hybrid functional approach is that it contains an empirical mixing-parameter  $\alpha$  (0.25 for HSE06) of the Hartree-Fock potential and an screening parameter  $\mu$  (0.2 for HSE06) to adjust the range of the spatial non-locality and to avoid the spin-density wave instability in the Hartree-Fock method.<sup>39,40</sup> This drawback has already been faced a lot of criticism of the less *ab initio* nature compared to the LDA/GGA

functional. To avoid this, we fixed  $\alpha = 0.25$  for all the screened hybrid functional calculations and we compare the screened hybrid functional results with quasi-particle GW results to determine the  $\mu$  parameter. Therefore, we have no free parameter in our screened hybrid functional calculations and our approach preserves the most valuable predictive power of *ab initio* method. It was shown that HSE06 share the same feature as QPGW in accounting for the electronic structures and lattice dynamical properties of the parent BaBiO<sub>3</sub> compound.<sup>41,42</sup>

Finally, if both frequency and momentum dependence are important in  $\Sigma(\omega, k)$ , there are strong local and non-local correlations. To treat the local and non-local correlations simultaneously, we need to combine the above methods such as GW+DMFT [43,44] and screened hybrid DFT+DMFT[45].

It has been established that the local correlation as seen in many partially filled *d*- and *f*-shell materials often have strong effects on lattice dynamical properties. For example, DMFT greatly improves LDA on the phonon spectra in Pu<sup>46</sup> and in the transition metal oxides MnO and NiO<sup>47</sup>. In the doped cuprate superconductors, the experimental width of the half-breathing phonon is about an order of magnitude larger than predicted by LDA calculations.<sup>48</sup>

In parallel, the screened hybrid functional has been shown to improve over LDA/GGA the phonon spectra of many materials including semiconductors<sup>49-51</sup>, oxides<sup>52</sup>, and molecules<sup>53</sup>. Note that the GW method and the (screened) hybrid functional are usually used to correct the underestimated LDA/GGA band gaps of some insulators and semiconductors. These approaches are generally believed to have little effects on or perform worse than LDA for metallic systems.<sup>40,54</sup> The impact of non-local correlation on the lattice dynamical properties and EPC of metallic materials has not been carefully studied.

In this paper, we will show that the non-local correlation can also have substantial impacts on the lattice dynamical properties of *metallic* materials where LDA/GGA strongly overscreens the electronic states, such as conducting materials in the vicinity of a metal-insulator transition (i.e., the parent compound is an insulator, while the doped compound become metallic upon sufficient doping). We find that the *screened* hybrid functional approach, when adjusted to match with QPGW results, is able to reproduce the experimental electronic structures and phonon frequencies of both the ‘‘other high temperature superconductors’’-the bismuthates and the transition metal chloronitrides for which LDA/GGA calculations show large discrepancies with experimental observations and a conventional high temperature superconductor MgB<sub>2</sub> for which LDA calculations show less discrepancies with experimental observations.

### III. EVALUATION OF ELECTRON-PHONON COUPLING

We now present our approach to evaluate the electron-phonon coupling. The EPC strength  $\lambda$  can be written as:<sup>55</sup> (the band index is omitted for simplicity)

$$\lambda = \frac{2}{N(\varepsilon_F)N_q} \sum_{k,q,\nu} |M_{k,k+q}^\nu|^2 \delta(\varepsilon_k) \delta(\varepsilon_{k+q}) / \omega_{q\nu} \quad (1)$$

where  $N_q$  is the number of  $q$  points,  $N(\varepsilon_F)$  is the total density of states per spin at the Fermi level  $\varepsilon_F$ ,  $\omega_{q,\nu}$  is the phonon frequency of branch  $\nu$  with wave vector  $q$ , and  $M_{k,k+q}^\nu$  are the electron-phonon matrix elements given by

$$M_{k,k+q}^\nu = \sum_j \left( \frac{\hbar^2}{2M_j \omega_{q\nu}} \right)^{1/2} \epsilon_{q,j}^\nu \cdot \langle k+q | \delta V / \delta u_{q,j}^\nu | k \rangle \quad (2)$$

where  $j$  runs over the atoms in the unit cell and  $\delta V / \delta u_{q,j}^\nu$  is the partial derivative of the total Kohn-Sham potential energy with respect to a given phonon displacement  $u_q^\nu$  of the  $j$ -th atom. For optical vibration modes, with a wave vector  $q$  commensurate with the lattice, the electron-phonon matrix element can be inferred from the shifts of the energy bands in a supercell calculation (frozen phonons), which we denote as reduced electron-phonon matrix element  $D_{k,q}^\nu$  (REPME). For states on the Fermi surface, the electron-phonon matrix elements can be read directly from the splitting of the energy bands resulting from the phonon displacements, which are shown in Fig. 3.

As we shall show later, the modifications in more advanced approaches of the Fermi surface, the density of states  $N(\varepsilon)$  and the corresponding phonon frequencies  $\omega_{q,\nu}$  compared to LDA are significantly smaller than those of the electron-phonon matrix elements. Hence, the electron-phonon matrix elements is the dominating factor differing the realistic  $\lambda$  from the LDA value. As a result the realistic EPC  $\lambda$  can be estimated from a LRT-LDA calculation by rescaling the LDA REPMEs to the actual values given by more advanced approaches while keeping the integral over  $k$  and  $q$  of Eq. 1 at the LDA level. Here the more advanced approach should be able to accurately reproduce the ground state properties (comparing to LDA). In practice, a good estimation is achieved by using both an advanced approach and LDA to evaluate the REPMEs for all the strongly coupled phonon modes (which can be seen in the LDA linear response calculation) at special points in the Brillouin zone:

$$\lambda_A = \sum_\nu \lambda_{A\nu} \simeq \sum_\nu \lambda_{L\nu} \langle |D_A^\nu|^2 \rangle / \langle |D_L^\nu|^2 \rangle \quad (3)$$

where we denote the advanced approach (such as GW and screened hybrid functional approaches) as A and LDA as L. If the enhancements in the REPMEs of all the strongly coupled branches are of comparable magnitude we can estimate  $\lambda_A$  by

$$\lambda_A \simeq \lambda_L \langle |D_A^\nu|^2 \rangle / \langle |D_L^\nu|^2 \rangle \quad (4)$$

We note that the accuracy of estimating the realistic EPC using the above method can be improved by including more phonon modes when more computing resource is available. Eventually, to achieve a more accurate evaluation of the realistic EPC, linear response technique should be implemented into GW and/or screened hybrid functional DFT.

## IV. COMPUTATIONAL DETAILS

### A. Method

The electronic structures are calculated using both the VASP[56] code with GGA(PBE)[57] and HSE06[38] exchange-correlation functionals and WIEN2k[58] code with GGA(PBE)[57] exchange-correlation functional. Linear response calculations are carried out using the LMTART[12,59] code with the ideal cubic structures (i.e., without distortions). The crystal structures are taken from Ref.60 for BaBiO<sub>3</sub> and Ref. 61 for BaPbO<sub>3</sub>. For VASP calculations, the PAW-PBE pseudopotential is used in both DFT-GGA and DFT-HSE calculations. The energy cutoff for the wavefunction is 400 eV. The results of GGA calculations from VASP are double checked with results from WIEN2k with GGA(PBE) exchange-correlation functional. In linear response calculations, a 32<sup>3</sup> k mesh is used to converge the electron charge density. The electron phonon coupling constant is obtained with a 8<sup>3</sup> q mesh with 35 independent q points in the irreducible Brillouin zone. We use virtual crystal approximation to simulate the doping effect in the linear response calculations.

For GW calculations, we use the self-consistent quasiparticle GW (scQPGW) as implemented in VASP. To ensure good convergence of the scQPGW calculations, we use an energy cutoff of 400 meV, 480 bands and 6×6×6 k-mesh for the 10-atom/cell (Ba,K)BiO<sub>3</sub> and 240 bands and 12×12×4 k-mesh for the 6-atom/cell Hf/ZrNCl compounds.

### B. Frozen phonon calculations

For the frozen-phonon calculations, we create supercells adaptive to the momentum  $Q$  of the phonon mode. For example, to calculate the oxygen breathing frequency at  $X$ ,  $M$  and  $R$  points in bismuthates, we create 2×1×1, 2×2×1, and 2×2×2 supercells of the simple cubic unit cell, respectively. Upon atomic displacement  $u$  of a phonon mode with wavevector  $Q$ , the phonon frequency is extracted as  $\omega = (E''(u)|_{u=0}/M_{eff})^{1/2}$  in the harmonic approximation, where  $M_{eff}$  is the effective mass and  $E(u)$  is the total energy as a function of the atomic displacement  $u$  in the DFT frozen phonon calculation. For instance, the effective mass  $M_{eff}$  is 6 times of oxygen atomic mass in calculating the oxygen breathing frequency at  $R$  point.

### C. Estimation of $\omega_{log}$

While  $\omega_{log}$  usually decreases with increasing  $\lambda$ , there isn't a simple relation between them. Following a discussion in Ref. [33], we estimate the HSE06 value  $\omega_{log,H}$  in optimal hole-doped BaBiO<sub>3</sub> (and other compounds in Table I of the main article) from the corresponding LDA value  $\omega_{log,L} \simeq 550$  K[13] via an empirical relation as  $\omega_{log,H} \simeq \omega_{log,L}(1 + \lambda_L)^{1/2}/(1 + \lambda_H)^{1/2} \simeq 450$  K which is in good agreement with the value about 450 K extracted from experiments[30,62]. The good agreement of the  $\omega_{log}$  in optimal hole-doped BaBiO<sub>3</sub> between the estimated HSE06 value and experimental value suggests, a) the above relation is a reasonable approximation and b) the HSE06  $\lambda_H$  is close to the realistic EPC in this material which further supports our view that HSE06 is appropriate for estimating the EPC in BaBiO<sub>3</sub>-related materials.

### D. Evaluating Coulomb pseudopotential

To estimate the Coulomb pseudopotential  $\mu^*$ , we implemented the methodology of Ref.[63] in our codes[64, 65] which combine LDA and GW methods in a linearized augmented plane-wave (LAPW) basis set.  $\mu^*$  is given by the formula

$$\mu^* = \frac{\mu}{1 + \mu \ln \frac{\varepsilon_F}{\omega_D}} \quad (5)$$

where  $\varepsilon_F$  is the Fermi energy and  $\omega_D$  the Debye energy, and dimensionless parameter  $\mu$  is calculated as the following average over Fermi surface

$$\mu = N(E_F) \frac{\sum_{\mathbf{k}\mathbf{k}'} \sum_{\lambda\lambda'} W_{\mathbf{k}\lambda;\mathbf{k}'\lambda'} \delta(\varepsilon_{\mathbf{k}\lambda} - E_F) \delta(\varepsilon_{\mathbf{k}'\lambda'} - E_F)}{\sum_{\mathbf{k}\mathbf{k}'} \sum_{\lambda\lambda'} \delta(\varepsilon_{\mathbf{k}\lambda} - E_F) \delta(\varepsilon_{\mathbf{k}'\lambda'} - E_F)}, \quad (6)$$

where  $N(E_F)$  is the density of states at Fermi level per spin,  $\varepsilon_{\mathbf{k}\lambda}$  is the Kohn-Sham eigenvalue of the  $\lambda$ th band at a wave vector  $\mathbf{k}$ , and matrix elements of the screened Coulomb interaction in a basis of LDA eigenstates are calculated as the following

$$W_{\mathbf{k}\lambda;\mathbf{k}'\lambda'} = \langle \mathbf{k}'\lambda' \uparrow, -\mathbf{k}'\lambda' \downarrow | W | \mathbf{k}\lambda \uparrow, -\mathbf{k}\lambda \downarrow \rangle. \quad (7)$$

The resulting  $\mu^*$  for the ideal BaBiO<sub>3</sub>, BaPbO<sub>3</sub> and LaPbO<sub>3</sub> compounds are 0.104, 0.117 and 0.119 respectively.

The difference between our work and Ref. 63 is that we use finite temperature formalism and approximate  $\delta$  function with the imaginary part of LDA Matsubara's Green's function

$$\delta(\varepsilon_{\mathbf{k}\lambda} - E_F) \approx \text{Im} \frac{1}{i\omega_0 + E_F - \varepsilon_{\mathbf{k}\lambda}}, \quad (8)$$

where  $\omega_0$  is the smallest positive Matsubara's frequency. The expression (8) becomes exact in the limit of zero

temperature. Technically we perform the following steps. First we calculate LDA one-electron spectrum and corresponding wave functions. It provides us with LDA Green's function. Then we evaluate LDA polarizability  $P_{LDA} = G_{LDA}G_{LDA}$ . The third step is to calculate screened interaction  $W = V + VP_{LDA}W$ , where  $V$  is bare Coulomb interaction. After the third step we are able to get the Coulomb pseudopotential parameter.

## V. BISMUTHATES

We first apply our method to the bismuthates  $Ba_{1-x}K_xBiO_3$  which was found to superconduct below 32 K in 1988.<sup>1</sup>

### A. Crystal Structure

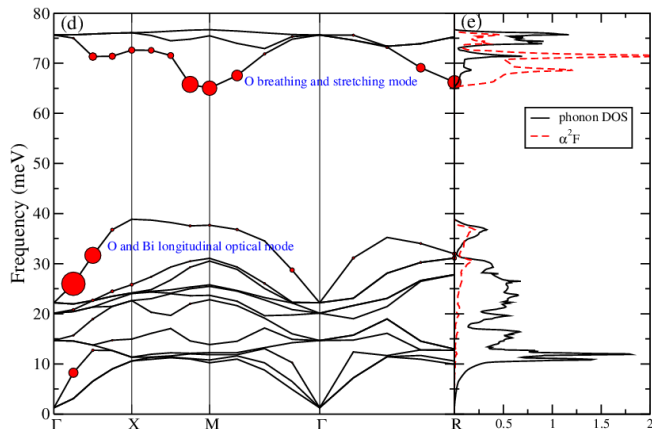
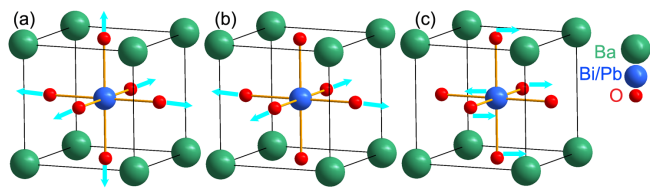


FIG. 1: (Color online) Top panel: Crystal structure of  $BaBiO_3$  and  $BaPbO_3$ . The arrows show (a) the oxygen breathing, (b) the oxygen stretching and (c) an oxygen and bismuth longitudinal optical vibration modes (the ferroelectric longitudinal optical mode). Bottom panel: (d) (left) phonon spectra and mode- and momentum  $q$ -dependent electron-phonon coupling strength  $\lambda_{q,\nu}$  (its value is proportional to the size of the circle at each  $q$  point) and (e) (right) the corresponding phonon density of states and the Eliashberg functional  $\alpha^2 F(\omega)$  of 0.4 hole doped  $BaBiO_3$ .

The optimal doped  $BaBiO_3$  (and  $BaPbO_3$ ) crystal-lize in the simple cubic perovskite structure as shown in Fig.1, whereas the parent compounds (without doping) display certain distortions from the ideal perovskite structure.<sup>60,61</sup> There are two types of distortions: one is

the oxygen breathing distortion along nearest-neighbor  $M-O$  bonds ( $M=Bi$  and  $Pb$ ) as shown in Fig. 1(a). The other one is the oxygen tilting distortion perpendicular to the nearest-neighbor  $M-O$  bonds (not shown). The oxygen breathing vibration was found to show strong EPC.<sup>13,66,67</sup>

### B. LDA linear response calculation

We first reproduce the LRT-LDA calculations of Ref. 13 and show the results in Fig. 1(d) and (e). We find that the oxygen breathing/stretching mode around  $R$  point (Fig.1(a)) and around  $M$  point (Fig.1(b)) dominate the contributions to the total  $\lambda$ , as evident from the mode- and momentum- dependent EPC  $\lambda_{q,\nu}$  shown in Fig.1(d) and the Eliashberg function  $\alpha^2 F(\omega)$  shown in Fig.1(e). In addition, we find at small  $q$  a longitudinal optical mode (so-called ferroelectric mode) depicted in Fig.1(c) which also has substantial EPC. These findings are in good agreement with previous observations as well.<sup>13,66,67</sup> On the contrary, acoustic phonon modes have very little contribution to the total EPC. With these findings, we argue that it is appropriate to use equation (3) to estimate the realistic EPC strength  $\lambda_A$  from LRT-LDA calculations in  $(Ba,K)BiO_3$ .

### C. Density of States

It was noted<sup>13</sup> that LDA suffers large discrepancies in describing the ground state properties of the parent compounds and some lattice dynamical properties of the metallic doped compounds in comparison with experiments. Recently, it was shown that a screened hybrid functional such as HSE06<sup>38</sup> largely removes the overscreening of LDA/GGA in the insulating (parent and lightly hole-doped)  $BaBiO_3$  compounds and describes many of their physical properties in excellent agreement with experiments.<sup>41,42</sup> It is however not clear if the screened hybrid functional also provides an improved description of the metallic hole-doped  $BaBiO_3$  compounds.

Here we show in Fig.2(a) the calculated density of states (DOS) of an optimal doped compound  $Ba_{0.62}K_{0.38}BiO_3$  using both the PBE functional and HSE06 functional in the DFT framework, and self-consistent quasiparticle GW method, based on virtual crystal approximation (VCA) and rigid band approximation (RBA), and we compare them with the experimental ultraviolet photoemission spectra[68] (UPS) of  $Ba_{0.62}K_{0.38}BiO_3$ . We note that the difference between RBA and the VCA is small with the PBE functional therefore only the RBA result is displayed in Fig.2(a). The HSE06 DOS is almost the same as the scQPGW DOS, and both of them have an overall good agreement with the experimental UPS, in particular they share roughly the same peak of the oxygen  $2p$  states centered at about -3.1 eV. In contrast, the DOS from PBE calcu-

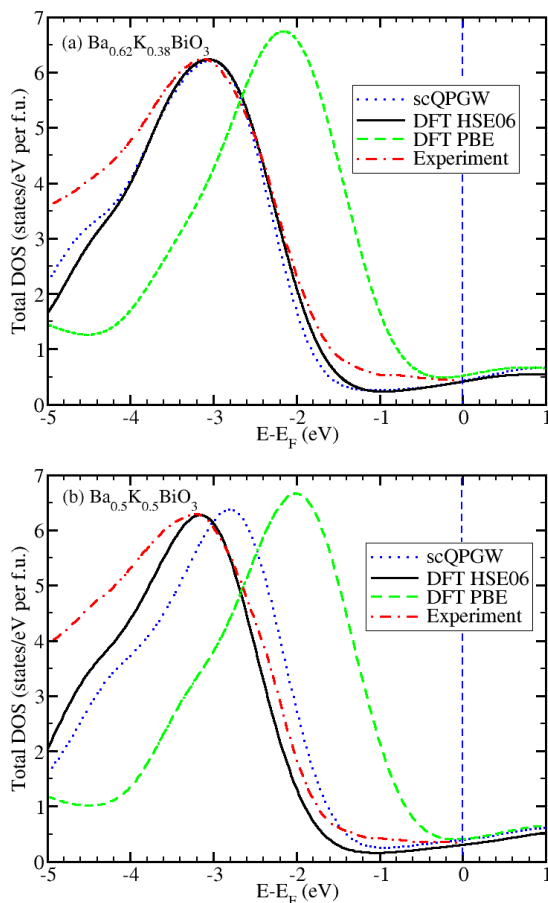


FIG. 2: **Density of states of  $\text{Ba}_{0.62}\text{K}_{0.38}\text{BiO}_3$  and  $\text{Ba}_{0.5}\text{K}_{0.5}\text{BiO}_3$ .** Top panel: the DOS of  $\text{Ba}_{0.62}\text{K}_{0.38}\text{BiO}_3$  calculated using the PBE functional, the HSE06 screened hybrid functional and the self-consistent quasiparticle GW, where doping is approximated with the rigid band approximation. Bottom panel: the DOS of  $\text{Ba}_{0.5}\text{K}_{0.5}\text{BiO}_3$  calculated using the PBE functional, the HSE06 screened hybrid functional and the self-consistent quasiparticle GW. Here the doping is simulated with a  $2 \times 2 \times 2$  supercell by substituting half of the Ba atoms with K atoms. The experimental data is the ultraviolet photoemission spectra for (a)  $\text{Ba}_{0.62}\text{K}_{0.38}\text{BiO}_3$  and (b)  $\text{Ba}_{0.52}\text{K}_{0.48}\text{BiO}_3$  taken from Ref. 68.

lation has a peak centered at about -2.2 eV, 0.9 eV away from the experimental position.

In Fig.2(b) we show the DOS for  $\text{Ba}_{0.5}\text{K}_{0.5}\text{BiO}_3$  calculated with PBE and HSE06 functionals, and scQPGW method. Instead of using VCA or RBA, we use a  $2 \times 2 \times 2$  supercell and replace half of the Ba atoms with K atoms to minimize errors induced by such approximations. We compare the results with the experimental UPS data for  $\text{Ba}_{0.52}\text{K}_{0.48}\text{BiO}_3$  from Ref.68. Again we find very good agreement between the HSE06 calculated DOS and experimental spectral. The peak position of the scQPGW DOS is 0.4 eV off the experimental one whereas the peak position of the PBE DOS is 1.2 eV off the experimental one.

Therefore, both the scQPGW method and HSE06 *screened* hybrid functional provide a significantly improved description of the electronic structures of the *metallic* (Ba,K)BiO<sub>3</sub> compounds compared to the LDA results, in strong contrast to the common belief that GW and hybrid functional are worse than LDA for metals.

#### D. Phonon frequencies

It is not feasible to compute the phonon frequencies using the scQPGW method currently. Here we provide evidence that HSE06 also improves the estimation of phonon-related quantities over LDA/GGA for the metallic (Ba,K)BiO<sub>3</sub> compounds. The scQPGW phonon frequencies are expected to be similar to the HSE06 results. We show in Table I the phonon frequencies of the oxygen breathing/stretching mode at  $X$ ,  $M$ ,  $R$  points and the so-called ferroelectric longitudinal optical phonon mode (see Fig.1) at  $\Gamma$  and  $X$  points in  $\text{BaKBi}_2\text{O}_6$  (a realistic K doping into  $\text{BaBiO}_3$ ) computed using the frozen-phonon method with both GGA and HSE06. We display also in Table I the phonon frequencies computed by DFT-GGA and LRT-LDA with the virtual crystal approximation (VCA) for  $\text{Ba}_{0.6}\text{K}_{0.4}\text{BiO}_3$  and  $\text{Ba}_{0.5}\text{K}_{0.5}\text{BiO}_3$  and compared with available experiments from Ref.69 for  $\text{Ba}_{0.6}\text{K}_{0.4}\text{BiO}_3$  and Ref.33 for  $\text{Ba}_{0.48}\text{K}_{0.52}\text{BiO}_3$ . For the oxygen breathing mode at  $M$  and  $R$  points, we find the HSE06 frequencies are in very good agreements with experimental data whereas GGA overestimates the experimental frequencies by about 10%. The HSE06 improves GGA on the oxygen breathing frequency at  $X$  point, where HSE06(GGA) overestimates the experimental value by 9%(21%). For the ferroelectric longitudinal optical mode, the phonon frequency at  $X$  point is similar in HSE06 and GGA as expected from the small  $\lambda_{q,\nu}$  shown in Fig.1. However, at  $\Gamma$  point, the HSE06 phonon frequency of this mode (18.1 meV) is considerably smaller than the GGA value (22.7 meV) due to the enhanced  $\lambda_{q,\nu}$  and is in good agreement with experimental observation ( $\sim 18$  meV)[33].

#### E. Band structures and reduced electron-phonon matrix elements

As an example, we show in Fig.3 the band structures of  $\text{BaBiO}_3$  with and without the oxygen breathing displacement (see Fig. 1(a)) to illustrate the huge differences in the REPME of the oxygen breathing mode at  $R$  point computed by GGA and HSE06. The band splittings indicated by the arrows in Fig.3 are about 1.17 eV for DFT-HSE06 and 0.67 eV for DFT-GGA, upon a displacement of  $0.044 \text{ \AA}$ , resulting in REPMEs of about 13.3 and 7.6 eV/ $\text{\AA}$ , respectively. We also compute this splitting using scQPGW under the same displacement. The corresponding value is 1.10 eV, resulting in a REPME of about 12.5 eV/ $\text{\AA}$ . The scQPGW results confirm again

TABLE I: Phonon frequencies of the important longitudinal optical phonon modes at high symmetry points in BaKBi<sub>2</sub>O<sub>6</sub> calculated by supercell frozen phonon calculations in the DFT-GGA and DFT-HSE06 framework. For comparison, the corresponding phonon frequencies from LRT-LDA calculations for Ba<sub>0.6</sub>K<sub>0.4</sub>BiO<sub>3</sub> and Ba<sub>0.5</sub>K<sub>0.5</sub>BiO<sub>3</sub> using the virtual crystal approximation (VCA), as well as from experimental measurements (exp.1 from Ref.69 and exp.2 from Ref.33) are also displayed.

Doping method	Q	DFT-GGA	DFT-HSE06	DFT-GGA	LRT-LDA	LRT-LDA	exp.1	exp.2
Mode/Doping $x$		K substitution	K substitution	VCA	VCA	VCA	K substitution	K substitution
Breathing	$R$	68.4	<b>61.2</b>	72.3	75.1	68.6	<b>62</b>	
	$M$	64.7	<b>59.0</b>	64.3	68.8	67.9	<b>60</b>	
	$X$	66.6	<b>60.1</b>	71.0	74.2	75.9	<b>55</b>	<b>55</b>
Ferroelectric	$\Gamma$	22.7	<b>18.1</b>	22.9	23.8	23.6	25	<b>18</b>
	$X$	37.2	<b>38.1</b>	38.6	39.7	39.7	<b>36</b>	<b>35</b>

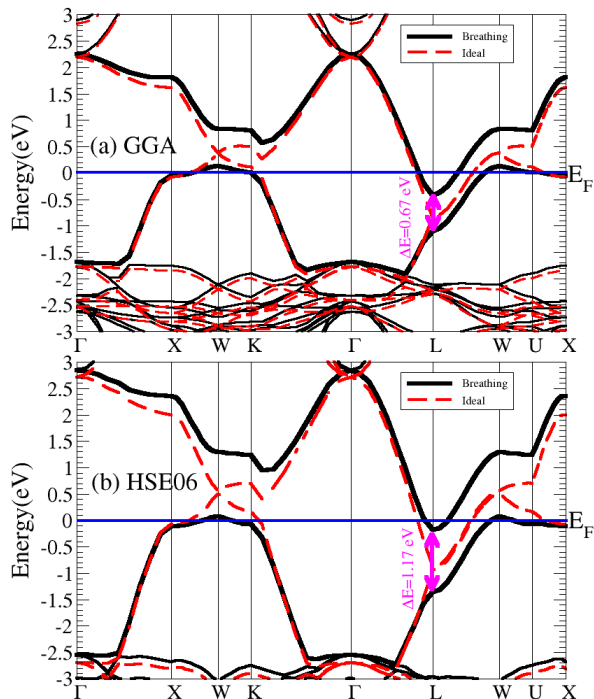


FIG. 3: (Color online) Illustration of the big REPME of the oxygen breathing mode at  $R$  point in BaBiO<sub>3</sub>. The band structures of BaBiO<sub>3</sub> with and without oxygen breathing displacement calculated by DFT using both the (a) GGA and (b) HSE06 hybrid functionals. We plot the band structure in the Brillouin zone of the  $fcc$  unit cell corresponding to a  $2 \times 2 \times 2$  supercell of the simple cubic unit cell due to the oxygen-breathing distortion. The displacement of each oxygen is about  $0.044 \text{ \AA}$  in the calculations. The band splittings indicated by the arrows are about  $1.17 \text{ eV}$  for DFT-HSE06 and  $0.67 \text{ eV}$  for DFT-GGA, resulting in REPMEs of about  $13.3$  and  $7.6 \text{ eV/\AA}$ , respectively. The corresponding scQPGW values are  $1.10 \text{ eV}$  and  $12.5 \text{ eV/\AA}$ , respectively. Note that the material remains metallic with the oxygen breathing distortion.

that HSE06 is applicable to the metallic (Ba,K)BiO<sub>3</sub> compounds. The above results indicate that the EPC strength for this mode is strongly enhanced by about a factor of three in the more accurate HSE06 and scQPGW treatments compared to the LDA value. Notice that the

material remains metallic with the oxygen breathing distortion, therefore the enhanced REPME in the HSE06 and scQPGW approaches compared to the LDA value is not merely a band gap problem of LDA.

We also compute the REPME of the oxygen breathing mode at  $R$  point (see Fig.4) in BaKBi<sub>2</sub>O<sub>6</sub> and find it to be about  $13.7$ ,  $11.0$ , and  $7.8 \text{ eV/\AA}$  in scQPGW, HSE06, and GGA, respectively. Notice again that the material remains metallic with the oxygen breathing distortion. Therefore, even in the overdoped Ba<sub>0.5</sub>K<sub>0.5</sub>BiO<sub>3</sub> compound, the EPC is strongly enhanced in scQPGW (HSE06), about a factor of three (two) of the LDA/GGA value, confirming that the effects of doping on the REPME is relatively weak. Hence, while the LDA/GGA quantitative overestimation of the phonon frequencies is less severe than its underestimation of the REPME, they are consistent manifestations of the overscreening problem of LDA/GGA and calculations with the HSE06 functional brings both quantities in closer agreement with experiments.

## F. Realistic electron-phonon coupling and $T_c$

To estimate the realistic EPC, we compute the REPMEs of the three most important phonon modes as suggested by LDA linear response calculations. These phonon modes are depicted in Fig. 1(a-c). The REPMEs of the oxygen breathing mode with  $Q$  vector corresponding to  $R$  point (Fig. 1(a)) have been discussed above, about  $13.3$ ,  $12.5$  and  $7.6 \text{ eV/\AA}$  in HSE06, scQPGW and GGA calculations, respectively. Since scQPGW has more or less the same results as HSE06 and GGA to calculate the REPMEs for the other two phonon modes (Fig. 1(b-c)), whose values are about  $8.9$  and  $5.7 \text{ eV/\AA}$  in HSE06 but only  $5.1$ , and  $3.4 \text{ eV/\AA}$  in GGA, respectively. For all the three important phonon modes, we have  $|D_H^\nu|^2/|D_L^\nu|^2 \simeq 3.0$ . Based on the LRT-LDA calculated EPC  $\lambda_L \simeq 0.33$ , we estimate the realistic electron phonon coupling  $\lambda_H \simeq 3.0\lambda_L \simeq 1.0$  for optimal hole-doped BaBiO<sub>3</sub>.

At low doping, the EPC is strong enough to drive the material to a polaronic state,<sup>41</sup> whereas for optimal doped BaBiO<sub>3</sub> (eg. Ba<sub>0.6</sub>K<sub>0.4</sub>BiO<sub>3</sub>), we expect the

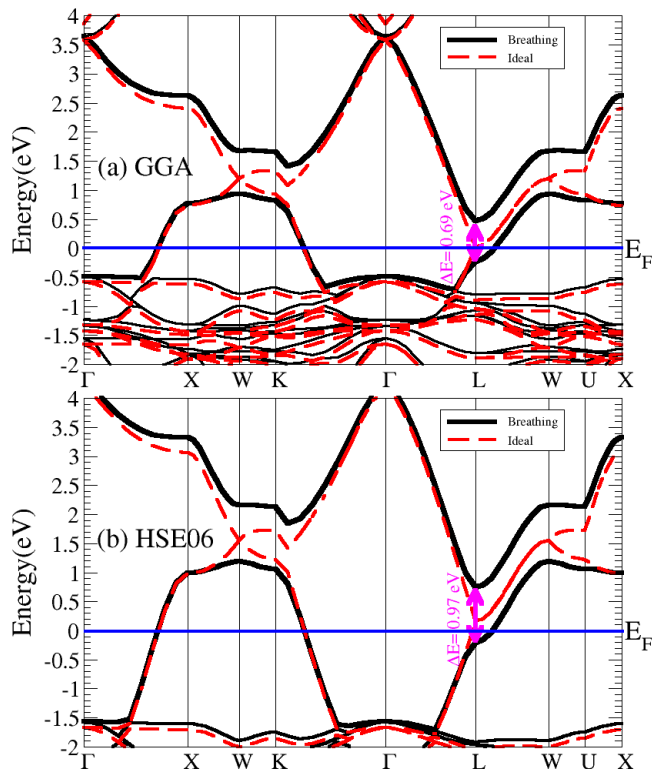


FIG. 4: (Color online) Illustration of the big REPME of the oxygen breathing mode at  $R$  in  $\text{BaKBi}_2\text{O}_6$ . The band structures of  $\text{BaKBi}_2\text{O}_6$  with and without oxygen breathing displacement calculated by DFT using both the (a) GGA and (b) HSE06 hybrid functionals. We plot the band structure in the Brillouin zone of the  $fcc$  unit cell corresponding to a  $2 \times 2 \times 2$  supercell of the simple cubic unit cell where half of the Ba atoms are replaced by K atoms. The displacement of each oxygen is about  $0.044 \text{ \AA}$  in the calculations. The band splittings indicated by the arrows are about  $0.97 \text{ eV}$  for DFT-HSE06 and  $0.69 \text{ eV}$  for DFT-GGA, resulting in REPMEs of about  $11.0$  and  $7.8 \text{ eV/\AA}$ , respectively. The corresponding sc-QPGW values are  $1.21 \text{ eV}$  and  $13.7 \text{ eV/\AA}$ , respectively. Note that the material remains metallic with the oxygen breathing distortion.

Migdal-Eliashberg theory is valid in this region. Using the modified McMillan equation

$$T_c = \frac{\omega_{log}}{1.20} \exp\left(-\frac{1.04(1 + \lambda)}{\lambda - \mu^*(1 + 0.62\lambda)}\right) \quad (9)$$

with estimated  $\omega_{log} \simeq 450 \text{ K}$  (see section III (C)) and  $\lambda = 1.0$ ,  $T_c$  is estimated to be  $31 \text{ K}$  (see Table VI) with  $\mu^* = 0.1$  which is the conventionally nominated value and is consistent with the value obtained by our first principles calculations as detailed in Section III (D). As a result, the strong EPC strength  $\lambda \simeq 1.0$  is enough to explain the high  $T_c \simeq 32 \text{ K}$  in K-doped  $\text{BaBiO}_3$  in the framework of a novel correlation-enhanced phonon mediated mechanism.

## G. Material and doping dependence of $T_c$

### 1. $\text{BaPbO}_3$

We note that the previous reasoning can also be used to estimate the EPC in one compound from another isostructural compound by comparing their REPMEs, provided that they have similar band structure around the Fermi level when optimally doped.

We also carried out LRT-LDA calculations in  $\text{Ba}_{1-x}\text{La}_x\text{PbO}_3$  based on virtual crystal approximation. We find a strong doping dependent  $\lambda_L$ , which is very small at small La doping and reaches a maximum value of  $0.58$  at  $x = 0.7$ . The EPC in optimally doped  $(\text{Ba},\text{La})\text{PbO}_3$  is thus estimated to be about  $0.58$  (LDA) and  $0.72$  (HSE06). Our calculation suggests superconductivity with  $T_c$  up to  $18 \text{ K}$  in optimally doped  $(\text{Ba},\text{La})\text{PbO}_3$  compound. (see Table VI) Experimentally  $11 \text{ K}$  superconductivity was found in a  $\text{Ba}_{1-x}\text{La}_x\text{PbO}_3$  multiphase compound synthesized at high pressure, but the crystal structure of the superconducting phase was not identified.<sup>70</sup> It would be very interesting to synthesize high-quality single-crystal  $\text{Ba}_{1-x}\text{La}_x\text{PbO}_3$  compound in the perovskite structure and test our theory.

### 2. $\text{Ba}_{n+1}\text{Bi}_n\text{O}_{3n+1}$

Our work sheds light on mystery of the dimensionality dependence of  $T_c$  in  $\text{BaBiO}_3$ -related materials. In heavy fermion materials, low dimensionality enhances superconductivity relative to their three dimensional versions.<sup>71</sup> On the other hand in  $\text{BaBiO}_3$ -related materials, layering, as in the synthesis of  $\text{Ba}_{n+1}\text{Bi}_n\text{O}_{3n+1}$  ( $n=1, 2, 3, \dots$ ) degrades  $T_c$ . We evaluate the REPME associated with O-breathing vibration and found it to be almost zero for the  $\text{Ba}_3\text{Bi}_2\text{O}_7$  compound ( $n=2$  member), resulting in very weak EPC and non-superconductivity, as seen in experiments<sup>72</sup>. While general factors may promote superconductivity in layered materials relative to their three dimensional version, a system specific calculation for the  $\text{BaBiO}_3$  family reveals that in this case the dominant effect is the reduction of the coupling of the phonon modes to the electrons in the two dimensional materials and this results in a reduction of  $T_c$ .

## VI. TRANSITION METAL CHLORONITRIDES

We turn to another member of the “other high temperature superconductors”: the electron-doped  $MNX$  ( $M=\text{Ti}, \text{Zr}, \text{ and Hf}$ ;  $\text{N}=\text{nitrogen}$ ;  $X=\text{Cl}, \text{Br}, \text{ and I}$ ). These materials are also proximate to an insulating state and their  $T_c$  are  $16.5, 16$  and  $25.5 \text{ K}$  for electron-doped  $\alpha\text{-TiNCl}$ ,  $\beta\text{-ZrNCl}$  and  $\beta\text{-HfNCl}$ , respectively.<sup>73,74</sup> A LRT-LDA calculation reported  $\lambda$  about  $0.52$  and  $\omega_{log}$  about  $36.4 \text{ meV}$  in  $1/6$  electron-doped  $\text{ZrNCl}$ ,<sup>14</sup> which gives  $T_c$  only  $6 \text{ K}$  (assuming  $\mu^*=0.1$ ) and is insufficient to account



for its 16 K superconductivity, raising again the question of what is the mechanism of superconductivity in this family.

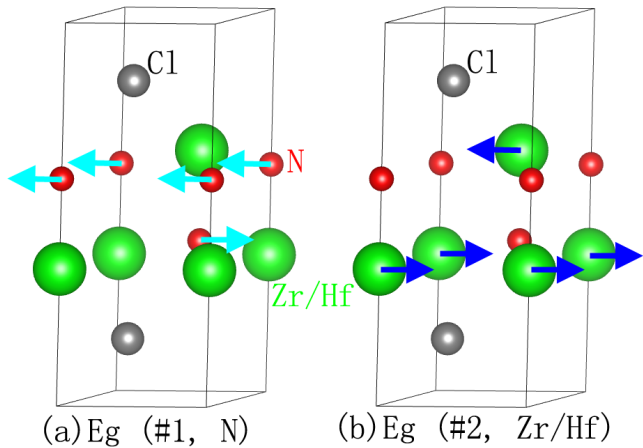


FIG. 5: (Color online) Simplified crystal structure of ZrNCl/HfNCl. The arrows show (a) the  $E_g$  mode with in-plane N vibration, (b)  $E_g$  mode with in-plane Zr/Hf vibration.

### A. Crystal Structure

ZrNCl and HfNCl crystallizes in a rhombohedral structure whose unit cell is built up with three neutral  $(\text{ZrNCl})_2$  units in a hexagonal structure. The neutral  $(\text{ZrNCl})_2$  units are connected *via* weak van der Waals force along the  $c$ -axis. Since the adjacent layers of the  $(\text{ZrNCl})_2$  units are weakly coupled, we ignore the shifting between the layers for simplicity, which results in a hexagonal unit cell (Space group  $P\bar{3}m1$ , #164, see Fig.5).

In Fig.5, we show two  $E_g$  vibration modes involving mainly in-plane vibrations of the nitrogen atoms (Fig.5(a)) and the Zr/Hf atoms (Fig.5(b)). For simplicity, we ignore the small vibrations of the rest atoms in each mode. Such a simplification has negligible influence on the calculated phonon frequencies as shall be shown in the following subsection.

We include in Table II the structural parameters used in our calculations for ZrNCl,  $\text{Li}_{0.25}\text{ZrNCl}$ , HfNCl and  $\text{Na}_{0.25}\text{HfNCl}$ . Note that we simplify the structure to a single layer of the  $(\text{Zr/HfNCl})_2$  unit. This simplification is expected to have little impact on the calculated electronic structures and lattice dynamics, due to the weak van der Waals force between the layers.

### B. Density of States

The scQPGW, DFT-HSE06 and DFT-GGA calculated total density of states for the parent ZrNCl and HfNCl

TABLE II: Crystal structures of ZrNCl,  $\text{Li}_{0.25}\text{ZrNCl}$ , HfNCl and  $\text{Na}_{0.25}\text{HfNCl}$  used in our calculations. The atomic positions are Zr/Hf:  $(0, 0, z(\text{Zr/Hf}))$  and  $(2/3, 1/3, -z(\text{Zr/Hf}))$ ; N:  $(0, 0, z(\text{N}))$  and  $(2/3, 1/3, -z(\text{N}))$ , and Cl:  $(1/3, 2/3, z(\text{Cl}))$  and  $(1/3, 2/3, -z(\text{Cl}))$ . Note in the space group  $P\bar{3}m1$ , the atomic positions are shifted to Zr/Hf:  $(2/3, 1/3, z(\text{Zr/Hf}))$  and  $(1/3, 2/3, -z(\text{Zr/Hf}))$ ; N:  $(2/3, 1/3, z(\text{N}))$  and  $(1/3, 2/3, -z(\text{N}))$ , and Cl:  $(0, 0, z(\text{Cl}))$  and  $(0, 0, -z(\text{Cl}))$ . Here we stick to the notation for the experimental structure.

Compound	$a$	$c$	$z(\text{Zr/Hf})$	$z(\text{N})$	$z(\text{Cl})$	exp.
ZrNCl	3.6046	9.224	0.3577	0.5931	0.1634	Ref. 75
$\text{Li}_{0.25}\text{ZrNCl}$	3.591	9.280	0.6379	0.4086	0.1655	Ref. 76
HfNCl	3.5767	9.237	0.3585	0.5928	0.1639	Ref. 75
$\text{Na}_{0.25}\text{HfNCl}$	3.5879	9.8928	0.6309	0.4110	0.1676	Ref. 77

compounds are shown in Fig. 6 and compared to available experiments reported in Ref. 78. While the overall shape of the DOS is similar in all the methods, the bandwidths of the valence states and the band gap between the valence states and conduction states differ substantially. We collect the valence bandwidths and the fundamental band gaps in Table III and compare to experimental values reported in Refs. 78,79. Clearly HSE06 account very well the valence bandwidths and band gaps in both materials, whereas GGA (scQPGW) underestimates (overestimates) the band widths by 0.5-0.7 eV (0.3-0.4 eV) and the fundamental band gaps by about 1.0 eV (0.5 eV).

Upon electron doping, except a shift of the chemical potential (Fermi energy), the overall DOS of  $\text{Na}_{0.25}\text{HfNCl}$  remains unchanged, as shown in Fig. 6(b), in consistent with experimental observations reported in Ref. 80. Here HSE06 functional again reproduces correctly the valence band width and the gap between the valence bands and conduction bands whereas GGA underestimates both quantities to similar magnitudes as in the parent compound. On the other hand, the calculated valence band widths in  $\text{Li}_{0.25}\text{ZrNCl}$  increases by about 0.7-0.8 eV compared to the parent compound ZrNCl, as shown in Fig. 6(a) and Table III. This observation is consistent with the trend seen in experiment [81] where the valence band widths in  $\text{Na}_{0.42}\text{ZrNCl}$  increases to about 7.0 eV. Note that HSE06 again gives better estimation of the valence band width than GGA in  $\text{Li}_{0.25}\text{ZrNCl}$ .

As a result, the electronic structures in both the parent and the electron doped ZrNCl and HfNCl are much better accounted for by DFT-HSE06 than DFT-GGA.

### C. Phonon frequencies

It was suggested<sup>14</sup> that the in-plane optical phonons ( $E_g$  mode) from vibrations of N and Zr atoms dominate the EPC in  $\text{Li}_{1/6}\text{ZrNCl}$ . We therefore compute the phonon frequencies at  $\Gamma$  and  $K$  points of two  $E_g$  modes involving the in-plane vibration of N and Zr/Hf atoms as shown in Fig.5 in ZrNCl,  $\text{Li}_{0.25}\text{ZrNCl}$ , HfNCl

TABLE III: The valence band widths and the fundamental band gaps in ZrNCl and HfNCl and their electron-doped compounds calculated using the DFT-GGA, DFT-HSE06, and scQPGW methods and compared with experiments[78–81]. The DFT-HSE06 reproduces accurately both the valence band widths and fundamental band gaps in both materials whereas DFT-GGA underestimates the band width by 0.5-0.7 eV and the band gap by about 1.0 eV. scQPGW overestimates the valence bandwidth by 0.3-0.4 eV and the band gap by 0.5 eV.

	Compounds	DFT-GGA	DFT-HSE06	scQPGW	exp.
Valence band width	ZrNCl	5.5	6.1	6.5	6.1 (Ref. 78)
	Li <sub>0.25</sub> ZrNCl	6.3	6.8		7.0 (Ref. 81 for Na <sub>0.42</sub> ZrNCl)
	HfNCl	5.8	6.3	6.6	6.3 (Ref. 78)
	Na <sub>0.25</sub> HfNCl	5.8	6.3		6.3 (Ref. 80 for Na <sub>0.22</sub> HfNCl)
Fundamental band gap	ZrNCl	1.6	2.5	3.1	2.5 (Ref. 79)
	HfNCl	2.0	3.1	3.7	3.2-3.4 (Ref. 78)

TABLE IV: Phonon frequencies of the  $E_g$  mode at zone center  $\Gamma$  point and zone boundary  $K$  point in the parent ZrNCl and HfNCl compounds and electron-doped Li<sub>0.25</sub>ZrNCl and Na<sub>0.25</sub>HfNCl compounds calculated by frozen phonon calculations in the DFT-GGA and DFT-HSE06 framework. For comparison, the corresponding phonon frequencies from LRT-LDA calculation in Ref. 14, SCDFRPA calculations in Ref. 15, as well as from two experimental measurements (exp.1 from Ref. 82 and exp.2 from Ref. 83) are also displayed. For electron doping, two Li/Na atoms are placed at (0, 0, 0) and (0.5, 0.5, 0) in the  $2 \times 2 \times 1$  supercell of the original unit cell. Notice the strong phonon softening of the N-N  $E_g$  mode near K point upon electron doping. This phonon softening is strongly enhanced in DFT-HSE06 treatment.

Compound	mode $E_g$	DFT-GGA			DFT-HSE06			LRT-LDA $\Gamma$	SCDFRPA $\Gamma$	exp.1 $\Gamma$	exp.2 $\Gamma$
		$\Gamma$	$K$	$\delta\omega$	$\Gamma$	$K$	$\delta\omega$				
ZrNCl	N-N	74.3	79.3	5.0	75.5	82.5	7.0	77.0	77.2	75.0	75.1
Li <sub>0.25</sub> ZrNCl	N-N	77.1	69.6	-7.5	76.7	61.9	-14.8	74.4/78.6	74.8	75.5	
	$\Delta\Omega$	2.8	-9.7	-12.5	1.2	-20.6	-21.8	-2.6/1.6	-2.4	0.5	
HfNCl	N-N	76.1	81.0	4.9	76.8	82.3	5.5		80.9		78.6
	Na <sub>0.25</sub> HfNCl	N-N	74.9	66.1	-8.8	74.9	61.1	-13.8		75.3	
	$\Delta\Omega$	-1.2	-14.9	-13.7	-1.9	-21.2	-19.3		-5.6		-2.1
ZrNCl	Zr-Zr	24.9	33.6	8.7	25.4	37.4	12.0	21.2	23.7	22.2	22.8
Li <sub>0.25</sub> ZrNCl	Zr-Zr	25.8	31.1	5.3	25.3	27.1	1.8	21.0/20.5	22.5	22.1	
	$\Delta\Omega$	0.9	-2.5	-3.4	-0.1	-10.3	-10.2	-0.2/-0.7	-1.2	-0.1	
HfNCl	Hf-Hf	18.2	24.4	6.2	18.7	25.1	6.4		20.6		19.4
Na <sub>0.25</sub> HfNCl	Hf-Hf	18.2	21.4	3.2	18.5	21.4	2.9		17.1		19.5
	$\Delta\Omega$	0.0	-3.0	-3.0	-0.2	-3.7	-3.5		-3.5		0.1

and Na<sub>0.25</sub>HfNCl using the frozen phonon method with both GGA and HSE06 functionals. The structural parameters used in our calculations are the same as in Table II. We using a  $2 \times 2 \times 1$  supercell to calculate the phonon frequencies at  $K$  points. The phonon frequencies in Li<sub>0.25</sub>ZrNCl (Na<sub>0.25</sub>HfNCl) are calculated using a  $2 \times 2 \times 1$  supercell where two Li (Na) atoms are placed at (0, 0, 0) and (0.5, 0.5, 0) in the supercell. The calculated phonon frequencies are shown in Table IV and compared with previous LRT-LDA calculation [14] and SCDFRPA calculation[15] and available experiments [82,83].

A few points can be drawn from our calculations:

1)The phonon frequencies at  $\Gamma$  points are similar in HSE06 and GGA and close to experimental values, in consistent with other theoretical studies[14,15].

2)Upon electron doping, both  $E_g$  phonon modes strongly softens along the  $\Gamma$ - $K$  direction. For the  $E_g$  phonon mode involving in-plane nitrogen vibration, the HSE06 (GGA) calculated phonon frequency at  $K$  point softens by 29/25 (16/18) percent or 21.8/19.3 meV (12.5/13.7 meV) compared to  $\Gamma$  point in ZrNCl/HfNCl upon 0.25/f.u. electron doping. The corresponding numbers are 40/19 (13/17) percent or 10.2/3.5 meV (3.4/3.0 meV) for the  $E_g$  mode

involving the in-plane Zr/Hf vibration.

3)The observed softening is not due to a change of the crystal structure induced by doping. As shown in Table V, we calculate the phonon frequencies with the crystal structures of Li<sub>0.25</sub>ZrNCl and Na<sub>0.25</sub>HfNCl but without doping the Li/Na atoms, and find they are similar to the corresponding values in the parent compounds of ZrNCl and HfNCl, respectively, i.e., we don't observe phonon softening at  $K$  point. Hence, the phonon softening is of electronic rather than structural origin.

Therefore we conclude that for the  $E_g$  phonon modes, 1) strong EPC occurs around the zone boundary  $K$  point but not the zone center  $\Gamma$  point, consistent with the LRT-LDA results reported in Ref. 14, and 2) HSE06 has much stronger EPC around  $K$  point than GGA. Our results suggest that while LDA/GGA produces reasonable phonon frequencies near  $\Gamma$  point, it overestimates the phonon frequencies around the zone boundary. This is consistent with the comparison of the LRT-LDA phonon DOS with the experimental one in Ref. 14 and can be tested by future experiments.

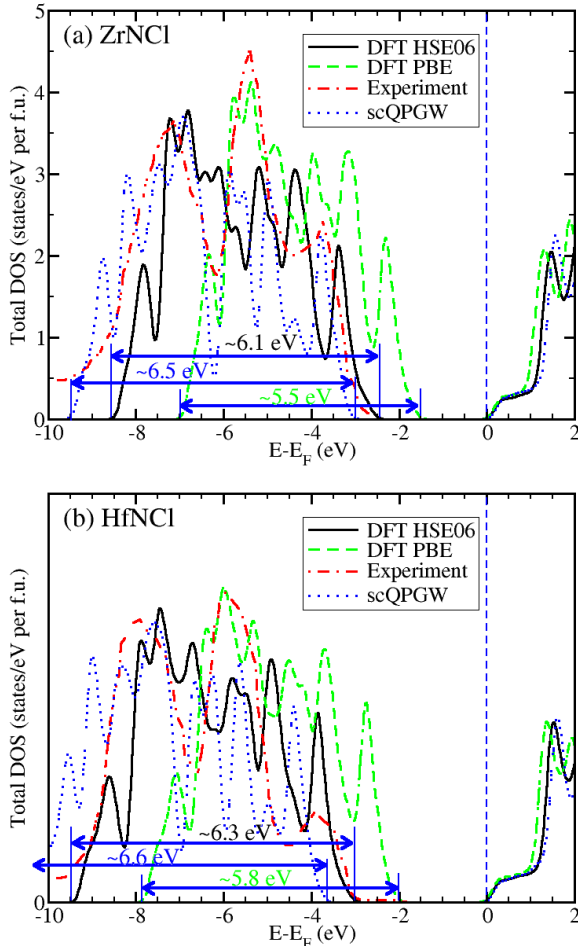


FIG. 6: Density of states of (a)ZrNCl and (b)HfNCl. The theoretical total DOS is calculated using the scQPGW method and the PBE functional and HSE06 hybrid functional within DFT . The experimental data is the photoemission spectra taken from Ref. 78.

#### D. Band structure and electron-phonon coupling

The DFT-PBE band structure and density of states of  $\beta$ -HfNCl is shown in Fig.8, which is calculated with its experimental crystal structure[75] without/Hf and/or N atoms shifted in the  $ab$  plane and along the  $c$ -axis to change the Hf-N bonding length. In the calculations, the experimental stacking of the layers along the  $c$ -axis is ignored for simplicity. Note that the study of Ref.14 used quite small electron doping (1/6), our calculations suggest at somewhat higher electron-doping the optical vibration of N and Zr atoms along  $c$  direction are also relevant to EPC. As the arrows indicated in the left panel of Fig.8, there are large REPMEs for the first two conduction bands, which are very flat along the  $\Gamma$ -A symmetry line, resulting in high density of states as shown in the right panel of Fig.8. Such high density of states makes electron-doping hardly change the chemical potential in this region.

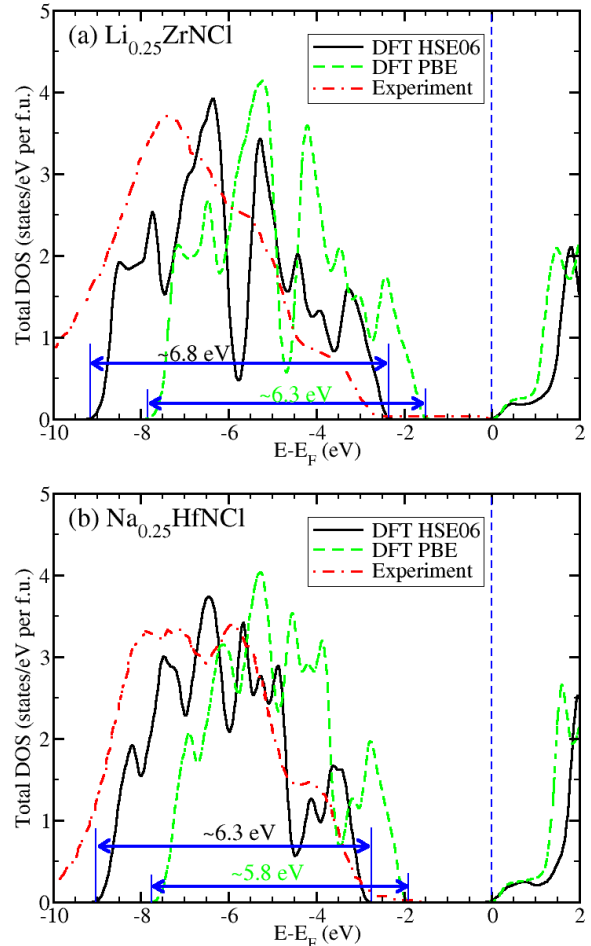


FIG. 7: Density of states of (a)Li<sub>0.25</sub>ZrNCl and (b)Na<sub>0.25</sub>HfNCl. The theoretical total DOS is calculated using both the PBE functional and HSE06 hybrid functional. Doping is approximated by placing two Li/Na atoms at (0, 0, 0) and (0.5, 0.5, 0) in the 2×2×1 supercell. The experimental data is the photoemission spectra taken from Ref. 81 for Na<sub>0.42</sub>ZrNCl and Ref. 80 for Na<sub>0.22</sub>HfNCl.

The study of Ref.14 suggests the EPC are mainly contributed by in-plane optical phonons ( $E_g$  mode) from vibrations of N and Zr atoms, with strong EPC near the zone boundary  $K$  point. We have shown that the experimental electronic structures of both parent and electron doped ZrNCl and HfNCl are much better reproduced by HSE06 than LDA. We also find that the phonon frequencies of the  $E_g$  mode soften more strongly in HSE06 than LDA near  $K$  point, similar to the oxygen breathing mode near the zone boundary points in (Ba,K)BiO<sub>3</sub>. The stronger softening of the HSE06  $E_g$  phonon frequencies is consistent with the comparison of the experimental and LRT-LDA phonon DOS shown in Ref. 14. It is therefore appropriate to use our approach (equation 3) to estimate the realistic EPC in this family. In the electron-doped  $\beta$ -ZrNCl compound, the REPMEs of the conduction bands associated with Zr-N vibrations in the plane and along  $c$

TABLE V: Phonon frequencies of the  $E_g$  mode at zone center  $\Gamma$  point and zone boundary  $K$  point in ZrNCl and HfNCl compounds with structures with/without electron doping calculated by frozen phonon calculations in the DFT-GGA and DFT-HSE06 framework. Notice that upon electron doping, the changes in the crystal structure don't cause substantial changes in the phonon frequencies. Therefore, the phonon softening shown in Table IV is electronic in origin rather than structural.

Compound	structure used	mode $E_g$	DFT-GGA			DFT-HSE06		
			$\Gamma$	$K$	$\delta\omega$	$\Gamma$	$K$	$\delta\omega$
ZrNCl	ZrNCl	N-N	74.3	79.3	5.0	75.5	82.5	7.0
	Li <sub>0.25</sub> ZrNCl	N-N	76.7	81.4	4.7	77.5	83.0	5.5
	$\Delta\Omega$	N-N	2.4	2.1	-0.3	2.0	0.5	-1.5
HfNCl	HfNCl	N-N	76.1	81.0	4.9	76.8	82.3	5.5
	Na <sub>0.25</sub> HfNCl	N-N	75.4	80.5	5.1	75.9	81.6	5.7
	$\Delta\Omega$	N-N	-0.7	-0.5	0.2	-0.9	-0.7	0.2
ZrNCl	ZrNCl	Zr-Zr	24.9	33.6	8.7	25.4	37.4	12.0
	Li <sub>0.25</sub> ZrNCl	Zr-Zr	26.1	34.6	8.5	26.5	35.4	8.9
	$\Delta\Omega$	Zr-Zr	1.2	1.0	-0.2	1.1	-2.0	-3.1
HfNCl	HfNCl	Hf-Hf	18.2	24.4	6.2	18.7	25.1	6.4
	Na <sub>0.25</sub> HfNCl	Hf-Hf	18.1	24.3	6.2	18.5	25.0	6.5
	$\Delta\Omega$	Hf-Hf	-0.1	-0.1	0.0	-0.2	-0.1	0.1

direction are substantially enhanced from 2.9-4.0 eV/Å in LDA to 3.9-4.7 eV/Å in HSE06. The enhanced REPME in HSE06 results in  $\lambda_H \sim 0.8$  and  $T_c=18$  K (see Table VI), in agreement with experimental value of 16.0 K. Interestingly, the enhanced electron-phonon coupling evaluated by DFT-HSE06 doesn't lead to a larger specific heat coefficient  $\gamma = \frac{2}{3}(1 + \lambda)\pi^2 k_B^2 N(0)$  compared to its DFT-LDA value because the electronic density of states at Fermi level, i.e.  $N(0)$ , is reduced in DFT-HSE06 by about 20% compared to DFT-LDA at the same time.

### E. Material and doping dependence of $T_c$

Our theory explains several counterintuitive experimental observations. It explains naturally the higher  $T_c$  in electron-doped  $\beta$ -HfNCl than electron-doped  $\beta$ -ZrNCl, despite the fact that the Hf atom is substantially heavier than Zr atom and therefore it would be expected to have lower frequency and lower  $T_c$  in a BCS picture. It turns out that the dominant factor governing the  $T_c$  is the value of the REPME which is substantially larger in  $\beta$ -HfNCl than in  $\beta$ -ZrNCl, and increased from 3.8-4.4 eV/Å in LDA to 5.1-5.3 eV/Å in HSE06. Since  $\beta$ -HfNCl is isostructural to  $\beta$ -ZrNCl, the enhanced REPME give  $\lambda_H \sim 1.1$  and  $T_c=25$  K for electron-doped  $\beta$ -HfNCl (see Table VI), in good agreement with experiment. The 16.5 K superconductivity in electron-doped  $\alpha$ -TiNCl[73] may also be well accounted for in the same way.

Another mystery in this family is the weak doping dependence of  $T_c$ , which is quite different from the trends in other known high temperature superconductors, including the BaBiO<sub>3</sub>-based ones where  $T_c$  depends crucially on the doping level. To understand this, notice that in

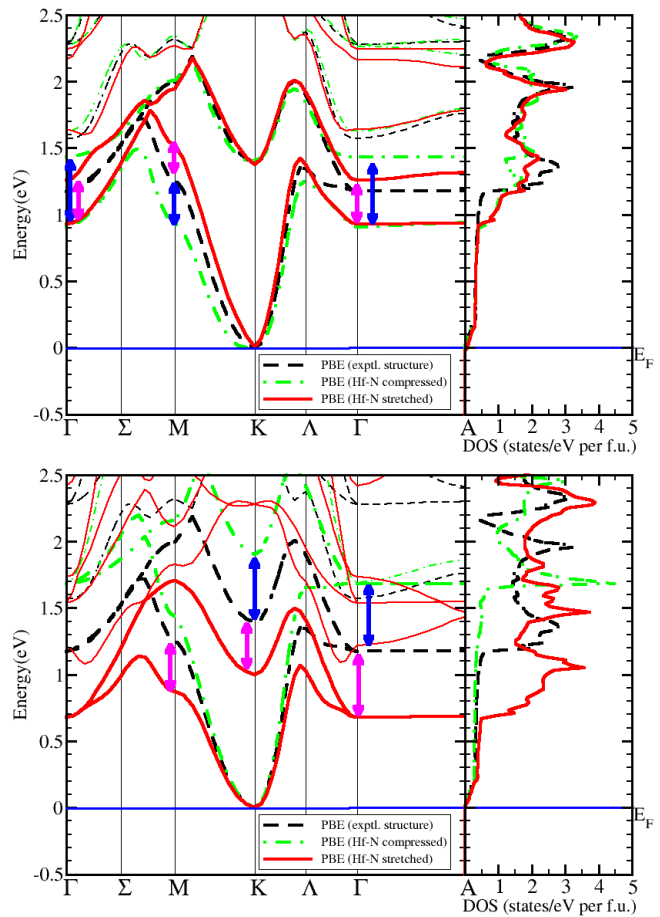


FIG. 8: **Band structure and density of states of  $\beta$ -HfNCl.** The band structure and density of states of  $\beta$ -HfNCl calculated using the PBE functional with the experimental crystal structure[75] and with the experimental crystal structure except the Hf and/or N atoms are shifted in the  $ab$  plane (top panel) and along the  $c$ -axis (bottom panel) such that the Hf-N bond is compressed or stretched by 0.09 Å. For simplicity, the different layer stacking along  $c$ -axis is ignored. Note the Fermi level is set to the bottom of the conduction band since we are interested in electron doping.

this family the conduction band as shown in Fig.8 has the largest REPMEs thus strong EPC at about 1.0 eV above the bottom of the conduction band. In the same energy region, this conduction band, being flat in certain parts of the Brillouin zone (along  $\Gamma - A$  for example), results in high density of states which makes the Fermi level hardly change with increasing doping level after some critical doping. The combination of the large REPMEs and high density of states in the same energy region is likely a plausible explanation of the weak doping dependence of  $T_c$  in the HfNCl family.

## VII. SUMMARY AND DISCUSSION

### A. Summary

Table VI summarizes our results on selected lattice dynamical properties (REPMEs,  $\omega_{log}$ ), the EPC and the  $T_c$  within the Migdal-Eliashberg theory for the materials studied above. Enhancements of the REPMEs in the more advanced and accurate HSE06 screened hybrid functional treatment and scQPGW method compared to LDA give rise to stronger EPC strengths and softening of strongly electron-phonon coupled phonon modes, consistent with many experimental observations as discussed above. The enhanced EPC and renormalized phonon frequency  $\omega_{log}$  readily account for the rather high temperature superconductivity in the doped bismuthates and transition metal chloronitrides within the Migdal-Eliashberg theory. In addition, using the important REPMEs, we can explain the material dependence of superconductivity, such as high  $T_c$  (up to 32 K) in (Ba,K)BiO<sub>3</sub>, intermediate  $T_c$  (<20 K) in (Ba,La)PbO<sub>3</sub> and Ba(Pb,Bi)O<sub>3</sub> and low  $T_c$  (<2K) in (Ba,K)<sub>3</sub>(Bi,Pb)<sub>2</sub>O<sub>7</sub>. We are also able to explain the material and doping dependence of  $T_c$  in  $A_x$ HfNCl and  $A_x$ ZrNCl ( $A$ =Li, Na, etc.)

### B. Two general sources of the underestimation of EPI by LDA

The underestimation of the EPI by LDA in materials close to a metal-insulator transition is very general, and is closely related to the failure of LDA in describing the ground state properties of the parent compounds. This can be understood intuitively as follows: LDA overestimates dielectric screening while the EPI is inversely proportional to the dielectric constant<sup>84</sup>, therefore the EPI strength is reduced in LDA relative to its true value.

The materials studied in this paper represent two general sources which cause the underestimation of the EPI by LDA. The first general source is the underestimation of the relevant band widths by LDA which causes an underestimation of the REPMEs. The transition metal chloronitrides represent this case where LDA underestimates the band width of the lowest conduction band by about 10% in the parent compounds and 20% in the 1/4 electron doped compounds compared the HSE06 treatment. (see Fig.6 and 7 for the first peak positions in the DOS of the conduction bands from GGA, HSE06, and/or scQPGW.) The second general source is the underestimation of the fundamental band gap by LDA, where the fundamental band gap is caused by atomic distortions. In this case the fundamental band gap is closely connected to the REPMEs of the corresponding atomic distortions. The bismuthates belong to the second case where the fundamental band gap is of indirect type and is only about 0.15 eV in LDA<sup>13</sup> while the experimental value is in the range of 0.5-0.9 eV<sup>85</sup>. Notice that the cor-

responding value in the HSE06 treatment is about 0.65 eV.<sup>41</sup>

### C. Screened and unscreened hybrid functionals: HSE06 vs B3LYP

There is much doubt on the applicability of hybrid functional to metallic materials partially because the famous B3LYP type hybrid functional fails in describing metallic systems. One reason is that the B3LYP functional fails to attain the exact homogeneous electron gas limit<sup>40</sup> due to the spin density wave instability in the Hartree-Fock method<sup>39</sup>. Paier, Marsman, and Kresse found that observing this limit is exceedingly important for extended systems.<sup>37,40</sup> On the other hand, the HSE-type *screened* functional has been designed to describe the homogeneous electron gas exactly therefore the HSE-type functional performs much better than the B3LYP functional.<sup>40</sup> Detailed comparisons of the performance of B3LYP and HSE-type functionals and other functionals are available in the literature (see for example, Refs. 40 and 54). For lattice dynamical properties, it was found that the B3LYP functional overestimate the EPI of some phonon modes in extended systems such as graphene and graphite,<sup>86</sup> whereas in the molecular systems such as C<sub>60</sub>, both the B3LYP and HSE-type functionals show similar improved estimation of the EPI.<sup>87,88</sup> Therefore, in the present paper we choose the *screened* hybrid functional HSE06 to study the doped bismuthates and transition metal chloronitrides, as they are extended metallic materials. The HSE06 functional is proven to be a good choice as it reproduces accurately the electronic structures and phonon frequencies of the considered materials.

### D. Screening parameter

In the construction of the HSE-type screened hybrid functional, it includes 1/4 of screened non-local exchange potential whose range is determined by a range-separation parameter  $\mu$ , where  $\mu=0$ , 0.2, and  $\infty$  corresponds to PBE0, HSE06, and PBE functional, respectively.<sup>54</sup> In more metallic materials, the HSE06 functional tends to overestimate the band widths and might perform worse than the conventional LDA functional.<sup>54</sup> To correct this issue of the HSE06 functional, the range-separation parameter  $\mu$  in the HSE-type functional has to be adjusted so as to get better agreements with the experimental or QPGW electronic structures in the normal state. We note that in the strongly overdoped region of the bismuthates and transition metal chloronitrides, the overscreening problem of LDA becomes less severe and the screening parameter in HSE06 functional has to be adjusted. Since the QPGW method can determine the degree of non-locality of the exchange-correlation potential self-consistently, the  $\mu$  parameter in the screened hybrid functional can be tuned

TABLE VI: REPME  $D$  (eV/Å) for the most important vibration mode, the total EPC  $\lambda$ , average phonon frequency  $\omega_{log}$  (K) and calculated  $T_c$  (K) in LDA and HSE06 are displayed with experimental  $T_c$  for selected compounds at optimal electron or hole doping.  $\omega_{log}$  in HSE06 is estimated from the corresponding LRT-LDA value as described in Section III. Critical temperatures in LDA and HSE06 are obtained from eq. (9) using  $\mu^*=0.10$ . (We concentrate on the dominating effect of  $\lambda$  and ignore the small variations in the values of  $\mu^*$  in the considered materials, which in practice affects the calculated  $T_c$  by a few Kelvins but doesn't affect our conclusions.) We approximate the LDA  $\omega_{log}$  for HfNCl to be about 80% of the value for ZrNCl according to the mass of Hf and Zr and their contribution to the total  $\lambda$  (about 40% according to Ref.14).

Compounds	mode	$D$ (LDA)	$D$ (HSE)	$\lambda$ (LDA)	$\lambda$ (HSE)	$\omega_{log}$ (LDA)	$\omega_{log}$ (HSE)	$T_c$ (LDA)	$T_c$ (HSE)	$T_c$ (exp.)
BaBiO <sub>3</sub>	O breathing at $R$	7.6	13.3	0.33	1.0	550	450	0.6	31	32.0 [1]
BaPbO <sub>3</sub>	O breathing at $R$	10.1	11.2	0.58	0.72	500	480	10.3	18	–
Ba <sub>3</sub> Bi <sub>2</sub> O <sub>7</sub>	O breathing at $R$	~0	~0	~0	~0	–	–	~0	~0	<2 [72]
ZrNCl	$E_g$ at $\Gamma$ (in-plane)	2.9-4.0	3.9-4.7	0.52	0.8	422	390	6.0	18	16 [74]
HfNCl	$E_g$ at $\Gamma$ (in-plane)	3.8-4.4	5.1-5.3		1.1	340	310	–	25	25.5 [2]

to fit the QPGW results. In this way, the  $\mu$  parameter in the screened hybrid functional can be determined by the QPGW method and is no longer an empirical parameter. Here we take MgB<sub>2</sub> as an example to demonstrate this. We show below that corrections beyond LDA/GGA are needed to better describe experimental observations in MgB<sub>2</sub>. By adjusting  $\mu$  in the HSE-type functional to fit the QPGW results, a modified HSE functional fixes the discrepancies between LDA/GGA and experiments and results in slightly stronger EPC strength and larger phonon linewidths, in consistent with the fact that LDA/GGA functional in average underestimates the experimental phonon line widths [89–92]. Therefore, the modified HSE functional provides a better estimation of the EPC strength in MgB<sub>2</sub>.

While LDA/GGA is commonly considered to be accurate for MgB<sub>2</sub>, there are various experimental observations are not well reproduced by LDA/GGA. For example, it was shown in Ref. 93 that LDA/GGA overestimated several de Haas-van Alphen frequencies by 200 T. For the smaller Fermi surface formed by the  $\sigma$  band in the  $\Gamma$  plane, LDA/GGA overestimated its size by 30 percent.[93] In the optical conductivity, the peak of the interband transition experimentally at about 2.6 eV was estimated to locate at about 2.4 eV by DFT-LDA/GGA.[94] That is to say, LDA/GGA underestimates the splitting between the lower  $\sigma$  band and the upper  $\pi$  band. These overestimations and underestimations of experimental observations by LDA/GGA suggest that corrections beyond LDA/GGA are needed to faithfully reproduce experimental results.

On the other hand, there are unexpectedly large discrepancies in the LDA/GGA results of the same quantity reported by different groups. For example, the de Haas-van Alphen frequencies of the same Fermi surfaces calculated by a few groups differ by 100-300 T.[93] Another example, the phonon frequency of the most important  $E_{2g}$  mode varies from 470-515 cm<sup>-1</sup>[95] to 585 cm<sup>-1</sup>[96] and to 575-665 cm<sup>-1</sup>[97]. Note the differences in the values of the reported frequencies in the preprint and published version of Ref. 95 and Ref. 97. These large discrepancies in the reported LDA/GGA results indicate unusual sensitive to the calculational details in MgB<sub>2</sub>.

In the following, we correct the above discrepancies between LDA/GGA and experiments in the optical conductivity and de Haas-van Alphen frequencies by using HSE-type screened hybrid functional and QPGW method. The range of the non-local exchange in the HSE type functional is adjusted by tuning the  $\mu$  parameter to fit the scQPGW results such as band structure (shown in Fig. 9) and DOS (shown in Fig. 10). In the calculations, we use experimental structure (lattice constants  $a = 3.0834$  and  $c = 3.5213$ , space group  $P6/mmm$ , #191) from Ref. 98.

In Table VII, we collect a few quantities calculated by DFT-GGA, DFT-HSE06 and DFT-mHSE (a modified HSE functional with  $\mu = 0.6$ ), scQPGW, and compare them with experimental values and previous theoretical calculations. The included quantities are the splitting  $\Delta E_{\sigma\pi}$  between the lower  $\sigma$  band and the  $\pi$  band around  $M$  point (marked as an arrow in Fig.9) showing as a interband transition peak in the optical conductivity, the de Haas-van Alphen frequency  $F_{\sigma\Gamma}$  of the lower  $\sigma$  band in the  $\Gamma$  plane, the phonon frequency  $\omega_{E_{2g}}$  of the  $E_{2g}$  mode, and the REPME (in eV/Å) of the  $E_{2g}$  mode.

Figure 9 shows the band structure of MgB<sub>2</sub> calculated by DFT-GGA, DFT-mHSE ( $\mu = 0.6$ ), and scQPGW. Consistent with previous LDA/GGA calculations as shown in Table VII, our DFT-GGA calculation also underestimates the splitting  $\Delta E_{\sigma\pi}$  by 0.2 eV and overestimates the de Haas-van Alphen frequency  $F_{\sigma\Gamma}$  by 190 T. On the contrary, DFT-HSE06 overestimates  $\Delta E_{\sigma\pi}$  by 0.4 eV and underestimates  $F_{\sigma\Gamma}$  by 190 T, suggesting HSE06 overcompensates the overscreening of LDA/GGA. Therefore we increase  $\mu$  to reduce the range of the non-local exchange potential in HSE06 functional. We find that a modified HSE type functional with  $\mu=0.6$  simultaneously fit well to the scQPGW results and reproduces the experimental  $\Delta E_{\sigma\pi}$ ,  $F_{\sigma\Gamma}$  and  $\omega_{E_{2g}}$  as shown in Table VII, Fig. 9 and Fig. 10. As a result, MgB<sub>2</sub> is a material sits between conventional metals which are well described by LDA/GGA functional and conventional insulators which are much better described by the HSE06 screened hybrid functional.

Since MgB<sub>2</sub> are better described by the mHSE functional with  $\mu=0.6$ , we now proceed to estimate the EPC

TABLE VII: Various quantities in MgB<sub>2</sub> calculated by DFT-GGA, DFT-HSE06, DFT-mHSE ( $\mu = 0.6$ ), scQPGW, and compared to available experiments, including the first interband transition peak position (in eV) in optics, de Haas-van Alphen frequency ( $F_{\sigma\Gamma}$  in T) from the Fermi surface formed by the lower  $\sigma$  band in the  $\Gamma$  plane, phonon frequency (in meV) of the  $E_{2g}$  mode, calculated reduced electron-phonon matrix element (in  $\text{eV}/\text{\AA}$ ) of the  $E_{2g}$  mode.

	DFT-GGA $\mu=\infty$	DFT-HSE06 $\mu=0.2$	DFT-mHSE $\mu=0.6$	scQPGW	exp.	other DFT-LDA/GGA
peak position $\Delta E_{\sigma\pi}$ (eV)	2.4	3.0	<b>2.6</b>	2.6	<b>2.6</b> (Ref. 94)	2.4 (Ref. 102)
de Haas-van Alphen frequency $F_{\sigma\Gamma}$ (T)	730	350	<b>580</b>		<b>535-546</b> (Ref. 93)	728-878 (Ref. 103-105)
phonon frequency $\omega_{E_{2g}}$ (meV)	71.8	66.0	<b>70.5</b>		<b>69.6-71.2</b> (Ref. 100)	58-83 (Refs. 95-97)
REPME of $E_{2g}$ mode ( $\text{eV}/\text{\AA}$ )	12.3	16.5	13.9			13 (Ref. 101)

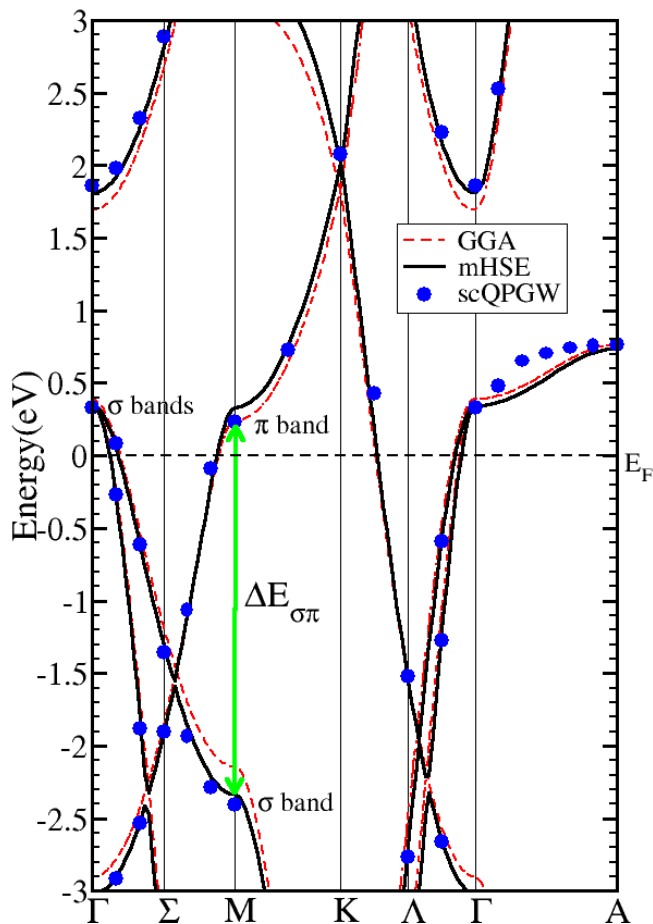


FIG. 9: Band structure of MgB<sub>2</sub> calculated by DFT-GGA and DFT-mHSE06, and QPGW. The DFT-mHSE ( $\mu=0.6$ ) band structure agrees well with that calculated by scQPGW, with a splitting of the  $\pi$  band and  $\sigma$  band at  $M$  point (i.e.,  $\Delta E_{\sigma\pi}$ ) about 2.6 eV, in good agreement with experiments<sup>94</sup>. DFT-GGA underestimates this splitting  $\Delta E_{\sigma\pi}$  by about 0.2 eV and overestimate the size of the  $\sigma$  Fermi surface centered at  $\Gamma$  point.

strength in MgB<sub>2</sub> combining the LRT-LDA  $\lambda$  and the frozen-phonon calculations. According to Ref. 96, the total LRT-LDA  $\lambda$  is about 0.87, of which  $\lambda_{\sigma}=0.62$  is contributed by the  $E_{2g}$  mode of the  $\sigma$  band and  $\lambda_{\pi}=0.25$  comes from the  $\pi$  band. Here we renormalize  $\lambda_{\sigma}$  and ignore the difference in  $\lambda_{\pi}$  because the latter makes a

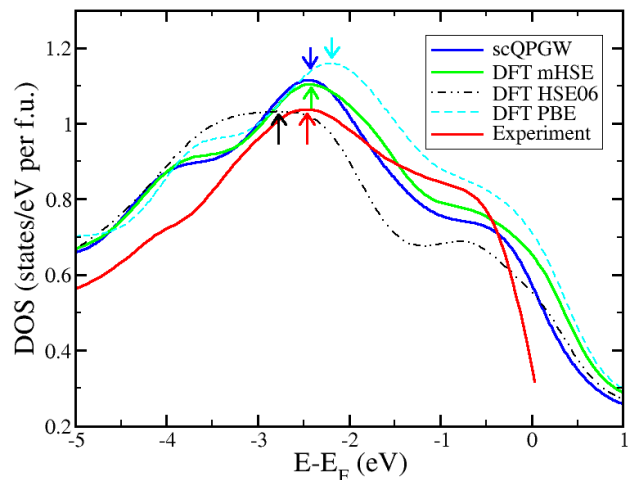


FIG. 10: Density of states of MgB<sub>2</sub> calculated by scQPGW, DFT-mHSE, DFT-HSE06, and DFT-GGA and compared to experiments<sup>99</sup>. For each DOS of all the data, an arrow is drawn to indicate the peak position which is mainly contributed by the B 2p states. The DOS of the scQPGW method, DFT-mHSE ( $\mu=0.6$ ) and experiment<sup>99</sup> share a common peak at about -2.4 eV whereas DFT-GGA underestimates this peak position by 0.2 eV (at about -2.2 eV) and DFT-HSE06 overestimates it by 0.4 eV (at about -2.8 eV).

much smaller contribution to the total EPC. The estimated EPC strength in mHSE functional is  $\lambda_{mHSE} = (13.9/12.3)^2 \lambda_{\sigma} + \lambda_{\pi} = 0.79 + 0.25 = 1.04$ , which is 0.17 bigger than the LRT-LDA value. This is consistent with the fact that LDA/GGA functional in average underestimates the experimental phonon line widths [89-92] and suggests that the mHSE functional provides a better estimation of the EPC strength in MgB<sub>2</sub>.

In short, MgB<sub>2</sub> is closer to a conventional superconductor than the bismuthates and transition metal chloronitrides. Applying the methodology we advocate in this paper, namely, using a screened hybrid functional and/or GW method that describes well the normal state properties to obtain an improved description of the superconducting state, does not lead to dramatic modifications of the existing picture for MgB<sub>2</sub>.

Although the difference between LDA/GGA and mHSE in MgB<sub>2</sub> is substantially smaller than in the case

of (Ba,K)BiO<sub>3</sub>, it is consistent manifestation of the overscreening problem of the LDA/GGA functional. It testifies our idea that due to the overscreening problem, LDA/GGA underestimates the EPC in these compounds. The realistic EPC thus has to be evaluated with a method which describes well the experimental electronic structures and phonon frequencies. In addition to the computational more demanding GW method, the HSE06 *screened* hybrid functional within DFT can serve as such a method for (Ba,K)BiO<sub>3</sub> and electron doped ZrNCl and HfNCl while a modified HSE-type *screened* hybrid functional within DFT is suitable for MgB<sub>2</sub>.

### E. Other materials

There is a class of materials where corrections beyond LDA/GGA are needed to account for the lattice dynamical properties and EPI. In addition to the doped bismuthates and transition metal chloronitrides, it was noted that in graphene<sup>86</sup> and organic molecular compounds, such as A<sub>3</sub>C<sub>60</sub><sup>87,88</sup> and picene<sup>106</sup>, GW or (screened) hybrid DFT methods are needed to evaluate phonon-related quantities. The latter two have narrow bands and may be in an antiadiabatic regime.<sup>107</sup> This class may include other puzzling materials such as Tl<sub>x</sub>PbTe<sup>108</sup> and undoubtedly many other systems still to be discovered.

## VIII. CONCLUSIONS

In conclusion, we show in this paper that first principles calculations based on LDA/GGA functional can significantly underestimate the EPI strength in certain materials where there are large non-local correlations such as materials in the vicinity of a metal-insulator transition. The doped BaBiO<sub>3</sub> and HfNCl family are such materials—the parent compounds are insulators while the sufficiently doped compounds are metals. This underestimation of EPI is caused by the overscreening of LDA/GGA in insulators, semiconductors and low-carrier bad metals, which results in an underestimation of the relevant band widths and/or the fundamental band gaps—two general sources of the underestimation of electron phonon coupling.

We present a simple but efficient method to evaluate the realistic EPC in these materials by combining the LDA linear response calculations and a few supercell calculations using a more advanced and accurate method such as GW and screened hybrid functional DFT which is able to provide a significantly improved description of normal state electronic structures and lattice dynamical properties of the materials compared to LDA.

We apply our method to evaluate the EPC in the doped BaBiO<sub>3</sub> and HfNCl family and find that the realistic electron phonon coupling are significantly enhanced over the LDA values and are strong enough to account for the rather high temperature superconductivity in these materials within the Migdal-Eliashberg theory. The puzzling discrepancies between theory and experiments in these materials are naturally resolved with our method. The “other high-temperature superconductors” such as those summarized in Refs.4,5 are thus strongly coupled superconductors where the coupling of the electrons to the lattice vibrations requires treatment of correlations beyond LDA/GGA.

Our method is also important for rational design of new superconductors and other EPI related functional materials through first principles calculations because determining the electron phonon coupling reliably is an essential step. As an example, we predict up to 18 K superconductivity in the perovskite Ba<sub>1-x</sub>La<sub>x</sub>PbO<sub>3</sub> compound around  $x = 0.7$ .

Our work suggests a critical reexamination of the realistic EPC is necessary in these and other materials such as the correlated cuprates and iron-based superconductors. Even in MgB<sub>2</sub> as discussed above, a careful reexamination shows LDA slightly underestimates the EPC.

Finally, we reiterate that our approach of estimating the realistic EPC can be improved by including more phonon modes and our work calls for implementing the linear response technique into GW and screened hybrid functional DFT to achieve a more accurate evaluation of the realistic EPC.

*Acknowledgments* We are grateful to Mac Beasley and Bob Cava for renewing our interest in this problem, and to Sergey Savrasov, Warren Pickett and Kristjan Haule for their useful comments. This work was supported by the AFOSR-MURI program.

---

\* Electronic address: yinziping@physics.rutgers.edu

<sup>1</sup> R. J. Cava, B. Batlogg, J. J. Krajewski, R. Farrow, L. W. Rupp Jr, A. E. White, K. Short, W. F. Peck, and T. Kometani, *Superconductivity near 30 K without copper: the Ba<sub>0.6</sub>K<sub>0.4</sub>BiO<sub>3</sub> perovskite*, Nature **332**, 814-816 (1988).

<sup>2</sup> S. Yamanaka, K.-I. Hotehama, and H. Kawaji, *Superconductivity at 25.5 K in electron-doped layered hafnium nitride*, Nature **392**, 580-582 (1998).

<sup>3</sup> O. Gunnarsson, *Superconductivity in fullerenes* Rev. Mod.

Phys. **69**, 575-606 (1997).

<sup>4</sup> W. E. Pickett, *The other high-temperature superconductors*, Physica B **296**, 112-119 (2001).

<sup>5</sup> W. E. Pickett, *The next breakthrough in phonon-mediated superconductivity*, Physica C **468**, 126-135 (2008).

<sup>6</sup> A. Taraphder, H. R. Krishnamurthy, R. Pandit, and T. V. Ramakrishnan, *Negative-U extended Hubbard model for doped barium bismuthates*, Phys. Rev. B **52**, 1368-1388 (1995).

<sup>7</sup> C. M. Varma, *Missing valence states, diamagnetic insula-*



- tors, and superconductors, Phys. Rev. Lett. **61**, 2713-2716 (1988).
- <sup>8</sup> W. Jin, M. H. Degani, R. K. Kalia, and P. Vashishta, *Superconductivity in  $Ba_{1-x}K_xBiO_3$* , Phys. Rev. B **45**, 5535-5546 (1992).
  - <sup>9</sup> T. M. Rice and L. Sneddon, *Real-space and  $\vec{k}$ -space electron pairing in  $BaPb_{1-x}Bi_xO_3$* , Phys. Rev. Lett. **47**, 689-692 (1981).
  - <sup>10</sup> G. Vielsack and W. Weber, *Search for negative  $U$  in the  $Ba_{1-x}K_xBi_{1-y}Pb_yO_3$  system using constrained density-functional theory*, Phys. Rev. B **54**, 6614-6623 (1996).
  - <sup>11</sup> W. A. Harrison, *Valence-skipping compounds as positive- $U$  electronic systems*, Phys. Rev. B **74**, 245128 (2006).
  - <sup>12</sup> S. Y. Savrasov, *Linear-response theory and lattice dynamics: a muffin-tin-orbital approach*, Phys. Rev. B **54**, 16470-16486 (1996).
  - <sup>13</sup> V. Mereghalli and S. Y. Savrasov, *Electron-phonon coupling and properties of doped  $BaBiO_3$* , Phys. Rev. B **57**, 14453-14469 (1998).
  - <sup>14</sup> R. Heid and K.-P. Bohnen, *Ab initio lattice dynamics and electron-phonon coupling in  $Li_xZrNCl$* , Phys. Rev. B **72**, 134527 (2005).
  - <sup>15</sup> R. Akashi, K. Nakamura, R. Arita, and M. Imada, *High-temperature superconductivity in layered nitrides  $\beta$ - $Li_xMNCl$  ( $M = Ti, Zr, Hf$ ): Insights from density functional theory for superconductors*, Phys. Rev. B **86**, 054513 (2012).
  - <sup>16</sup> W. E. Pickett, R. E. Cohen, and H. Krakauer, *Lattice instabilities, isotope effect, and high- $T_c$  superconductivity in  $La_{2-x}Ba_xCuO_4$* , Phys. Rev. Lett. **67**, 228-231 (1991).
  - <sup>17</sup> H. Krakauer, W. E. Pickett, and R. E. Cohen, *Large calculated electron-phonon interactions in  $La_{2-x}M_xCuO_4$* , Phys. Rev. B **47**, 1002-1015 (1993).
  - <sup>18</sup> A. Lanzara *et al.*, *Evidence for ubiquitous strong electron-phonon coupling in high-temperature superconductors*, Nature **412**, 510-514 (2001).
  - <sup>19</sup> T. Cuk, D. H. Lu, X. J. Zhou, Z.-X. Shen, T. P. Devereaux, and N. Nagaosa, *A review of electron-phonon coupling seen in the high- $T_c$  superconductors by angle-resolved photoemission studies (ARPES)*, Phys. Stat. Sol. (B) **242**, 11-29 (2005).
  - <sup>20</sup> O. Gunnarsson, and O. Rösch, *Interplay between electron-phonon and Coulomb interactions in cuprates*, J. Phys.: Condens. Matter **20**, 043201 (2008).
  - <sup>21</sup> S. M. Shapiro, G. Shirane, and J. D. Axe, *Measurements of the electron-phonon interaction in Nb by inelastic neutron scattering*, Phys. Rev. B **12**, 4899-4908 (1975).
  - <sup>22</sup> M. G. Mitch, S. J. Chase, and J. S. Lannin, *Raman scattering and electron-phonon coupling in  $Rb_xC_{60}$* , Phys. Rev. Lett. **68**, 883-886 (1992).
  - <sup>23</sup> E. L. Wolf, J. Zasadzinski, G. B. Arnold, D. F. Moore, J. M. Rowell, and M. R. Beasley, *Tunneling and the electron-phonon-coupled superconductivity of  $Nb_3Sn$* , Phys. Rev. B **22**, 1214-1217 (1980).
  - <sup>24</sup> O. Gunnarsson, H. Handschuh, P. S. Bechthold, B. Kessler, G. Ganteför, and W. Eberhardt, *Photoemission Spectra of  $C_{60}^-$ : Electron-Phonon Coupling, Jahn-Teller Effect, and Superconductivity in the Fullerenes*, Phys. Rev. Lett. **74**, 1875-1878 (1995).
  - <sup>25</sup> K. Prassides, C. Christides, M. J. Rosseinsky, J. Tomkinson, D. W. Murphy, and R. C. Haddon, *Neutron Spectroscopy and Electron-Phonon Coupling in Alkali-Metal-Doped Fullerenes*, Europhys. Lett. **19**, 629 (1992).
  - <sup>26</sup> D. Kasinathan, J. Kuneš, A. Lazicki, H. Rosner, C. S. Yoo, R. T. Scalettar, and W. E. Pickett, *Superconductivity and lattice instability in compressed lithium from Fermi surface hot spots*, Phys. Rev. Lett. **96**, 047004 (2006).
  - <sup>27</sup> Z. P. Yin, S. Y. Savrasov, and W. E. Pickett, *Linear response study of strong electron-phonon coupling in yttrium under pressure*, Phys. Rev. B **74**, 094519 (2006).
  - <sup>28</sup> Z. P. Yin, F. Gygi, and W. E. Pickett, *Competing phases, strong electron-phonon interaction, and superconductivity in elemental calcium under high pressure*, Phys. Rev. B **80**, 184515 (2009).
  - <sup>29</sup> Y. Kong, O. V. Dolgov, O. Jepsen, and O. K. Andersen, *Electron-phonon interaction in the normal and superconducting states of  $MgB_2$* , Phys. Rev. B **64**, 020501(R) (2001).
  - <sup>30</sup> N. Tralshawala, J. F. Zasadzinski, L. Coffey, W. Gai, M. Romalis, Q. Huang, R. Vaglio, and K. E. Gray, *Tunneling,  $\alpha^2F(\omega)$ , and transport in superconductors: Nb, V, VN,  $Ba_{1-x}K_xBiO_3$ , and  $Nd_{1.85}Ce_{0.15}CuO_4$* , Phys. Rev. B **51**, 3812-3819 (1995).
  - <sup>31</sup> M. A. Green, K. Prassides, D. A. Neumann, and P. Day, *Lattice Dynamics of Semiconducting, Metallic, and Superconducting  $Ba_{1-x}K_xBiO_3$  Studied by Inelastic Neutron Scattering*, Chem. Mater. **7**, 888-893 (1995).
  - <sup>32</sup> H. Khosroabadi, J. Kobayashi, K. Tanaka, S. Miyasaka, S. Tajima, H. Uchiyama and A. Q. R. Baron, *Softening of Bond Stretching Phonon Mode in  $Ba_{1-x}K_xBiO_3$  Superconductor*, J. Supercond. Nov. Magn. **23**, 1385-1389 (2010).
  - <sup>33</sup> H. Khosroabadi, S. Miyasaka, J. Kobayashi, K. Tanaka, H. Uchiyama, A. Q. R. Baron, and S. Tajima, *Softening of bond-stretching phonon mode in  $Ba_{1-x}K_xBiO_3$  at the metal-insulator transition*, Phys. Rev. B **83**, 224525 (2011).
  - <sup>34</sup> A. J. Cohen, P. Mori-Sánchez, and W. T. Yang, *Insights into current limitations of density functional theory*, Science **321**, 792-794 (2008).
  - <sup>35</sup> A. Georges, G. Kotliar, W. Krauth, and M. J. Rozenberg, *Dynamical mean-field theory of strongly correlated fermion systems and the limit of infinite dimensions*, Rev. Mod. Phys. **68**, 13 (1996).
  - <sup>36</sup> G. Kotliar, S. Y. Savrasov, K. Haue, V. S. Oudovenko, O. Parcollet, and C. A. Marianetti, *Electronic structure calculations with dynamical mean-field theory*, Rev. Mod. Phys. **78**, 865 (2006).
  - <sup>37</sup> T. M. Henderson, J. Paier, G. E. Scuseria, *Accurate treatment of solids with the HSE screened hybrid*, Phys. Status Solidi B **248**, 767774 (2011).
  - <sup>38</sup> A. V. Krukau, O. A. Vydrov, A. F. Izmaylov, and G. E. Scuseria, *Influence of the exchange screening parameter on the performance of screened hybrid functionals*, J. Chem. Phys. **125**, 224106 (2006).
  - <sup>39</sup> A. W. Overhauser, *Spin Density Waves in an Electron Gas*, Phys. Rev. **128**, 14371452 (1962).
  - <sup>40</sup> J. Paier, M. Marsman, and G. Kresse, *Why does the B3LYP hybrid functional fail for metals*, J. Chem. Phys. **127**, 024103 (2007).
  - <sup>41</sup> C. Franchini, G. Kresse, and R. Podloucky, *Polaronic Hole Trapping in Doped  $BaBiO_3$* , Phys. Rev. Lett. **102**, 256402 (2009).
  - <sup>42</sup> C. Franchini, A. Sanna, M. Marsman, and G. Kresse, *Structural, vibrational, and quasiparticle properties of the Peierls semiconductor  $BaBiO_3$ : a hybrid functional and self-consistent GW+vertex-corrections study*, Phys. Rev.

- B **81**, 085213 (2010).
- <sup>43</sup> P. Sun and G. Kotliar, *Extended dynamical mean-field theory and GW method*, Phys. Rev. B **66**, 085120 (2002).
- <sup>44</sup> S. Biermann, F. Aryasetiawan, and A. Georges, *First-Principles Approach to the Electronic Structure of Strongly Correlated Systems: Combining the GW Approximation and Dynamical Mean-Field Theory*, Phys. Rev. Lett. **90**, 086402 (2003).
- <sup>45</sup> D. Jacob, K. Haule and G. Kotliar, *Combining the hybrid functional method with dynamical mean-field theory*, EPL **84**, 57009 (2008).
- <sup>46</sup> X. Dai, S. Y. Savrasov, G. Kotliar, A. Migliori, H. Ledbetter, and E. Abrahams, *Calculated Phonon Spectra of Plutonium at High Temperatures*, Science **300**, 953-955 (2003).
- <sup>47</sup> S. Y. Savrasov and G. Kotliar, *Linear Response Calculations of Lattice Dynamics in Strongly Correlated Systems*, Phys. Rev. Lett. **90**, 056401 (2003).
- <sup>48</sup> O. Rösch and O. Gunnarsson, *Electron-Phonon Interaction in the  $t$ - $J$  Model*, Phys. Rev. Lett. **92**, 146403 (2004) and references therein.
- <sup>49</sup> K. Hummer, J. Harl, and G. Kresse, *Heyd-Scuseria-Ernzerhof hybrid functional for calculating the lattice dynamics of semiconductors*, Phys. Rev. B **80**, 115205 (2009).
- <sup>50</sup> J. Wróbel, K. J. Kurzydowski, K. Hummer, G. Kresse, and J. Piechota, *Calculations of ZnO properties using the Heyd-Scuseria-Ernzerhof screened hybrid density functional*, Phys. Rev. B **80**, 155124 (2009).
- <sup>51</sup> L. Qin, Y. Duan, H. Shi, L. Shi, and G. Tang *Hybrid density functional theory studies of AlN and GaN under uniaxial strain*, J. Phys.: Condens. Matter **25** 045801 (2013).
- <sup>52</sup> J. Graciani *et al.*, *Comparative Study on the Performance of Hybrid DFT Functionals in Highly Correlated Oxides: The Case of CeO<sub>2</sub> and Ce<sub>2</sub>O<sub>3</sub>*, J. Chem. Theory Comput. **7**, 56-65 (2011).
- <sup>53</sup> Y. Okamoto, M. Saito, and A. Oshiyama, *Hybrid density-functional study of the vibrational frequency of a H<sub>2</sub> molecule at the tetrahedral site of silicon*, Phys. Rev. B **58**, 7701-7706 (1998).
- <sup>54</sup> M. Marsman, J. Paier, A. Stroppa and G. Kresse, *Hybrid functionals applied to extended systems*, J. Phys.: Condens. Matter **20**, 064201 (2008).
- <sup>55</sup> P. B. Allen, *Neutron Spectroscopy of Superconductors*, Phys. Rev. B **6**, 2577 (1972).
- <sup>56</sup> G. Kresse and J. Furthmüller, *Efficiency of ab-initio total energy calculations for metals and semiconductors using a plane-wave basis set*, Comput. Mater. Sci. **6**, 15-50 (1996).
- <sup>57</sup> J. P. Perdew, K. Burke, and M. Ernzerhof, *Generalized gradient approximation made simple*, Phys. Rev. Lett. **77**, 3865-3868 (1996).
- <sup>58</sup> P. Blaha, K. Schwarz, G. K. H. Madsen, D. Kvasnicka, and J. Luitz, *WIEN2K An augmented plane wave + local orbitals program for calculating crystal properties*, (K. Schwarz, Techn. Univ. Wien, Austria, 2001).
- <sup>59</sup> S. Y. Savrasov and D. Y. Savrasov, *Electron-phonon interactions and related physical properties of metals from linear-response theory*, Phys. Rev. B **54**, 16487-16501 (1996).
- <sup>60</sup> D. E. Cox and A. W. Sleight, *Mixed-valent Ba<sub>2</sub>Bi<sup>3+</sup>Bi<sup>5+</sup>O<sub>6</sub>: structure and properties vs temperature*, Acta Cryst. **B35**, 1-10 (1979).
- <sup>61</sup> W. T. Fu, D. Visser, and D. J. W. IJdo, *High-resolution neutron powder diffraction study on the structure of BaPbO<sub>3</sub>*, Solid State Commun. **134**, 647-652 (2007).
- <sup>62</sup> C.-K. Loong, P. Vashishta, R. K. Kalia, W. Jin, M. H. Degani, D. G. Hinks, D. L. Price, J. D. Jorgensen, B. Dabrowski, A. W. Mitchell, D. R. Richards, and Y. Zheng, *Phonon density of states and oxygen-isotope effect in Ba<sub>1-x</sub>K<sub>x</sub>BiO<sub>3</sub>*, Phys. Rev. B **45**, 8052-8064 (1992).
- <sup>63</sup> K.-H. Lee, K. J. Chang, and M. L. Cohen, *First-principles calculations of the Coulomb pseudopotential  $\mu^*$ : application to Al*, Phys. Rev. B **52**, 1425-1428 (1995).
- <sup>64</sup> A. L. Kutepov and S. G. Kutepova, *The ab initio ground state properties and magnetic structure of plutonium*, J. Phys.: Condens. Matter **15**, 2607-2624 (2003).
- <sup>65</sup> A. Kutepov, S. Y. Savrasov, and G. Kotliar, *Ground-state properties of simple elements from GW calculations*, Phys. Rev. B **80**, 041103 (2009).
- <sup>66</sup> L. F. Mattheiss and D. R. Hamann, *Electronic structure of BaPb<sub>1-x</sub>Bi<sub>x</sub>O<sub>3</sub>*. Phys. Rev. B **28**, 4227-4241 (1983).
- <sup>67</sup> M. Shirai, N. Suzuki, and K. Motizuki, *Electron-lattice interaction and superconductivity in BaPb<sub>1-x</sub>Bi<sub>x</sub>O<sub>3</sub> and Ba<sub>x</sub>K<sub>1-x</sub>BiO<sub>3</sub>*, J. Phys.: Condens. Matter **2**, 3553-3566 (1990).
- <sup>68</sup> H. Namatame, A. Fujimori, H. Torii, T. Uchida, Y. Nagata, and J. Akimitsu, *Effects of hole doping and electron-phonon interaction on the electronic structure of Ba<sub>1-x</sub>K<sub>x</sub>BiO<sub>3</sub> studied by photoemission spectroscopy*, Phys. Rev. B **50**, 13674-13678 (1994).
- <sup>69</sup> M. Braden, W. Reichardt, A. S. Ivanov, and A. Yu. Rumiantssev, *Anomalous dispersion of LO phonon branches in Ba<sub>0.6</sub>K<sub>0.4</sub>BiO<sub>3</sub>*, Europhys. Lett. **34**, 531-536 (1996).
- <sup>70</sup> A. P. Menushenkov, A. V. Tsvyashchenko, D. V. Eremenko, K. V. Klementev, A. V. Kuznetsov, V. N. Trofimov and L. N. Fomichev, *Superconductivity in the Ba<sub>1-x</sub>La<sub>x</sub>PbO<sub>3</sub> system*, Phys. Solid State **43**, 613-615 (2001).
- <sup>71</sup> P. Monthoux and G. G. Lonzarich, *Magnetically mediated superconductivity: crossover from cubic to tetragonal lattice*, Phys. Rev. B **66**, 224504 (2002).
- <sup>72</sup> R. J. Cava, T. Siegrist, W. F. Peck, Jr., J. J. Krajewski, B. Batlogg, and J. Rosamilla, *(Ba,K)<sub>3</sub>Bi<sub>2</sub>O<sub>7</sub>: a layered bismuth oxide*, Phys. Rev. B **44**, 9746-9748 (1991).
- <sup>73</sup> S. Yamanaka, T. Yasunaga, K. Yamaguchi, and M. Tagawa, *Structure and superconductivity of the intercalation compounds of TiNCl with pyridine and alkali metals as intercalants*, J. Mater. Chem. **19**, 2573-2582 (2009).
- <sup>74</sup> S. Yamanaka, *High-T<sub>c</sub> superconductivity in electron-doped layer structured nitrides*, Annu. Rev. Mater. Sci. **30**, 53-82 (2000).
- <sup>75</sup> X.-A. Chen, T. Koiwasaki, and S. Yamanaka, *High-pressure synthesis and crystal structures of  $\beta$ -MNCl (M=Zr and Hf)*, J. Solid State Chem. **159**, 80-86 (2001).
- <sup>76</sup> X.-A. Chen, L.-P. Zhu, and S. Yamanaka, *The first single-crystal X-ray structural refinement of the superconducting phase Li<sub>0.2(1)</sub>ZrNCl derived by intercalation*, J. Solid State Chem. **169**, 149-154 (2002).
- <sup>77</sup> J. Oró-Solé, C. Frontera, B. Martínez, D. Beltrán-Porter, M. R. Palacn, and A. Fuertes, *A new intermediate intercalate in superconducting sodium-doped hafnium nitride chloride*, Chem. Commun. 3352-3354 (2005).
- <sup>78</sup> A. Ino, K. Yamazaki, T. Yamasaki, M. Higashiguchi, K. Shimada, H. Namatame, M. Taniguchi, T. Oguchi, X. Chen, and S. Yamanaka, *Angle-resolved-photoemission study of layer-structured nitride  $\beta$ -HfNCl*, Journal of Electron Spectroscopy and Related Phenomena **144-147**, 667-669 (2005).

- <sup>79</sup> T. Yokoya, T. Takeuchi, S. Tsuda, T. Kiss, T. Higuchi, S. Shin, K. Iizawa, S. Shamoto, T. Kajitani, and T. Takahashi, *Valence-band photoemission study of  $\beta$ -ZrNCl and the quasi-two-dimensional superconductor  $\text{Na}_x\text{ZrNCl}$* , Phys. Rev. B **70**, 193103 (2004).
- <sup>80</sup> T. Yokoya, Y. Ishiwata, S. Shin, S. Shamoto, K. Iizawa, T. Kajitani, I. Hase, and T. Takahashi, *Changes of electronic structure across the insulator-to-metal transition of quasi-two-dimensional Na-intercalated  $\beta$ -HfNCl studied by photoemission and x-ray absorption*, Phys. Rev. B **64**, 153107 (2001).
- <sup>81</sup> T. Yokoya, T. Takeuchi, S. Tsuda, T. Kiss, T. Higuchi, S. Shin, K. Iizawa, S. Shamoto, T. Kajitani, and T. Takahashi, *Valence-band photoemission study of  $\beta$ -ZrNCl and the quasi-two-dimensional superconductor  $\text{Na}_x\text{ZrNCl}$* , Phys. Rev. B **70**, 200501 (2004).
- <sup>82</sup> P. Adelman, B. Renker, H. Schober, M. Braden and F. Fernandez-Diaz, *Lattice Dynamics of Li-ZrNCl: An Electron doped Layered Superconductor*, J. Low Temp. Phys. **117**, 449 (1999).
- <sup>83</sup> A. Cros, A. Cantarero, D. Beltrán-Porter, J. Oró-Solé, and A. Fuertes, *Lattice dynamics of superconducting zirconium and hafnium nitride halides*, Phys. Rev. B **67**, 104502 (2003).
- <sup>84</sup> P. B. Allen and B. Mitrovic, **Theory of Superconducting Tc**. in *Solid State Physics* **37**, 1-92 (Academic Press, New York, 1982).
- <sup>85</sup> H. Namatame, A. Fujimori, H. Takagi, S. Uchida, F. M. F. de Groot, and J. C. Fuggle, *Electronic structure and the metal-semiconductor transition in  $\text{BaPb}_{1-x}\text{Bi}_x\text{O}_3$  studied by photoemission and x-ray-absorption spectroscopy*, Phys. Rev. B **48**, 16917-16925 (1993).
- <sup>86</sup> M. Lazzeri, C. Attaccalite, L. Wirtz, and F. Mauri, *Impact of the electron-electron correlation on phonon dispersion: Failure of LDA and GGA DFT functionals in graphene and graphite*, Phys. Rev. B **78**, 081406(R) (2008).
- <sup>87</sup> C. Faber, J. L. Janssen, M. Côté, E. Runge, and X. Blase, *Electron-phonon coupling in the  $\text{C}_{60}$  fullerene within the many-body GW approach*, Phys. Rev. B **84**, 155104 (2011).
- <sup>88</sup> J. L. Janssen, M. Côté, S. G. Louie, and M. L. Cohen, *Electron-phonon coupling in  $\text{C}_{60}$  using hybrid functionals*, Phys. Rev. B **81**, 073106 (2010).
- <sup>89</sup> A. Shukla, M. Calandra, M. dAstuto, M. Lazzeri, F. Mauri, C. Bellin, M. Krisch, J. Karpinski, S. M. Kazakov, J. Jun, D. Daghero, and K. Parlinski, *Phonon Dispersion and Lifetimes in  $\text{MgB}_2$* , Phys. Rev. Lett. **90**, 095506 (2003).
- <sup>90</sup> A. Q. R. Baron, H. Uchiyama, Y. Tanaka, S. Tsutsui, D. Ishikawa, S. Lee, R. Heid, K.-P. Bohnen, S. Tajima, and T. Ishikawa, *Kohn Anomaly in  $\text{MgB}_2$  by Inelastic X-Ray Scattering*, Phys. Rev. Lett. **92**, 197004 (2004).
- <sup>91</sup> A. Q. R. Baron, H. Uchiyama, R. Heid, K. P. Bohnen, Y. Tanaka, S. Tsutsui, D. Ishikawa, S. Lee, and S. Tajima, *Two-phonon contributions to the inelastic x-ray scattering spectra of  $\text{MgB}_2$* , Phys. Rev. B **75**, 020505(R) (2007).
- <sup>92</sup> M. dAstuto, M. Calandra, S. Reich, A. Shukla, M. Lazzeri, F. Mauri, J. Karpinski, N. D. Zhigadlo, A. Bossak, and M. Krisch, *Weak anharmonic effects in  $\text{MgB}_2$ : A comparative inelastic x-ray scattering and Raman study*, Phys. Rev. B **75**, 174508 (2007).
- <sup>93</sup> J. R. Cooper, A. Carrington, P. J. Meeson, E. A. Yelland, N.E. Hussey, L. Balicas, S. Tajima, S. Lee, S. M. Kazakov, and J. Karpinski, *de Haasvan Alphen effect in  $\text{MgB}_2$  crystals*, Physica C **385**, 75-84 (2003).
- <sup>94</sup> V. Guritanu, A. B. Kuzmenko, D. van der Marel, S. M. Kazakov, N. D. Zhigadlo, and J. Karpinski, *Anisotropic optical conductivity and two colors of  $\text{MgB}_2$* , Phys. Rev. B **73**, 104509 (2006).
- <sup>95</sup> J. Kortus, I. I. Mazin, K. D. Belashchenko, V. P. Antropov, and L. L. Boyer, *Superconductivity of Metallic Boron in  $\text{MgB}_2$* , Phys. Rev. Lett. **86**, 4656 (2001); arXiv:cond-mat/0101446.
- <sup>96</sup> Y. Kong, O. V. Dolgov, O. Jepsen, and O. K. Andersen, *Electron-phonon interaction in the normal and superconducting states of  $\text{MgB}_2$* , Phys. Rev. B **64**, 020501(R) (2001).
- <sup>97</sup> G. Satta, G. Profeta, F. Bernardini, A. Continenza, and S. Massidda, *Electronic and structural properties of superconducting  $\text{MgB}_2$ ,  $\text{CaSi}_2$ , and related compounds*, Phys. Rev. B **64**, 104507 (2001); arXiv:cond-mat/0102358.
- <sup>98</sup> M. E. Jones and R. E. Marsh, *The Preparation and Structure of Magnesium Boride,  $\text{MgB}_2$* , J. Am. Chem. Soc. **76**, 1434-1436 (1954).
- <sup>99</sup> T. A. Callcott, L. Lin, G. T. Woods, G. P. Zhang, J. R. Thompson, M. Paranthaman, and D. L. Ederer, *Soft-x-ray spectroscopy measurements of the p-like density of states of B in  $\text{MgB}_2$  and evidence for surface boron oxides on exposed surfaces*, Phys. Rev. B **64**, 132504 (2001).
- <sup>100</sup> W. X. Li, Y. Li, R. H. Chen, R. Zeng, M. Y. Zhu, H. M. Jin, and S. X. Dou, *Electron-phonon coupling properties in  $\text{MgB}_2$  observed by Raman scattering*, J. Phys.: Condens. Matter **20**, 255235 (2008).
- <sup>101</sup> J. M. An and W. E. Pickett, *Superconductivity of  $\text{MgB}_2$ : covalent bonds driven metallic*, Phys. Rev. Lett. **86**, 4366-4369 (2001).
- <sup>102</sup> A. B. Kuzmenko, F. P. Mena, H. J. A. Molegraaf, D. van der Marel, B. Gorshunov, M. Dressel, I. I. Mazin, J. Kortus, O. V. Dolgov, T. Muranaka, and J. Akimitsu, *Manifestation of multiband optical properties of  $\text{MgB}_2$* , Solid State Commun. **121**, 479-484 (2002).
- <sup>103</sup> I.I. Mazin and J. Kortus, *Interpretation of the de Haasvan Alphen experiments in  $\text{MgB}_2$* , Phys. Rev. B **65**, 180510(R) (2002).
- <sup>104</sup> H. Rosner, J. M. An, W. E. Pickett, and S. L. Drechsler, *Fermi surfaces of diborides:  $\text{MgB}_2$  and  $\text{ZrB}_2$* , Phys. Rev. B **66**, 024521 (2002).
- <sup>105</sup> H. Harima, *Energy band structures of  $\text{MgB}_2$  and related compounds*, Physica C **378-381**, 18-24 (2002).
- <sup>106</sup> G. Giovannetti and M. Capone, *Electronic correlation effects in superconducting picene from ab initio calculations*, Phys. Rev. B **83**, 134508 (2011).
- <sup>107</sup> M. Capone, M. Fabrizio, C. Castellani, and E. Tosatti, *Colloquium: Modeling the unconventional superconducting properties of expanded  $\text{A}_3\text{C}_{60}$  fullerenes*, Rev. Mod. Phys. **81**, 943 (2009).
- <sup>108</sup> Y. Matsushita, H. Bluhm, T. H. Geballe, and I. R. Fisher, *Evidence for Charge Kondo Effect in Superconducting Tl-Doped PbTe*, Phys. Rev. Lett. **94**, 157002 (2005).